3
UWB Antenna

UWB technology attracts the attention of researcher from academia and industry after the legalization of 7.5 GHz (3.1-10.6 GHz) bandwidth by FCC for UWB wireless communication system in 2002. Design and analysis of UWB antenna is more challenging compared to narrowband antennas due to three reasons. Firstly, it should have a wide operational bandwidth as specified by FCC. Secondly, it has to be small and compact with desired antenna characteristics because of its easy integration with UWB systems. Thirdly, it must have a good time-domain characteristics because UWB system uses short pulses of large bandwidth to transfer the information. The objective of this chapter is to design and investigate several compact fractal UWB antennas, in order to understand the various design aspects of fractal UWB antenna.

3.1 Introduction

The rapid development in modern wireless communication system put several challenges to the researchers. The modern wireless communication systems required high data transmission capacity, low power consumption, ease of fabrication, low cost and stable radiation pattern and others. The UWB antennas have the data transmission capacity of above 200 Mbps in the few meters range. Moreover, it transmits data at very low power levels, by spreading the transmitted signal over the UWB operating bandwidth 3.1–10.6 GHz [Amin *et al.*, 2012] and hence battery life of the device will be increased. Such developments in antenna design may provide several advantages over conventional data transmission in case of indoor communications. Hence, a compact UWB antenna has to be designed very carefully to enhance the system performance.

The application of fractal geometry in UWB antenna design helps to accomplish the above requirements. Fractal antenna is a combination of antenna technology and fractal geometry. The fractal antenna not only reduces the effective area, but also provides the multiple resonance phenomena simultaneously due to its self-similarity and space filling properties [Guterman *et al.*, 2004; Werner *et al.*, 1999; Ding *et al.*, 2007; Hashemi *et al.*, 2006]. The space filling property is used to miniaturize the antenna size by increasing the effective electrical path length [Anguera *et al.*, 2005; Hashemi *et al.*, 2006]. Moreover, the fractal geometries such as Koch snowflake [Anguera *et al.*, 2005], Sierpinski triangle [Werner *et al.*, 1999; Anguera *et al.*, 2005], hexagonal shaped [Werner *et al.*, 1999], Pythagorean tree [Pourahmadazar *et al.*, 2011], Koch [Patnam, 2008; Omar *et al.*, 2013], Cantor set [Li, Y.S. *et al.*, 2011] and Giusepe Peano [Oraizi and Hedayati, 2011] are used to design UWB antenna. In these different geometrical shaped fractal antennas, a small part of the geometry is repeated in a self-similar manner. As the number of iteration increases, the lower resonant frequency of antenna decreases due to increase in the effective electrical path length. The monopole/radiator shows efficient electromagnetic radiation because of discontinuities and bends present in the fractal structure [Anguera *et al.*, 2005]. These bends and discontinuities cause for the change in the current path, which in turn leads to enhance the radiation characteristics of the antenna [Balanis, 2005].

It is demonstrated that by etching rectangular [Zaker *et al.*, 2008; Amiri *et al.*, 2012] or L-shaped [Zaker *et al.*, 2009] slots in the ground plane, fractional bandwidth up to 125% is

achieved. However, most of these antennas are large in dimensions, which make them difficult to integrate with commercial devices. Thus, these techniques are not very efficient for compact wideband antennas. The application of fractal geometry in UWB antenna design helps to accomplish the above requirements. Therefore, fractal antenna is a promising topic and needs to be genuinely investigated and developed.

3.2 Ultra Wideband (UWB) Antenna Using Minkowski Like Fractal Geometry

3.2.1 Antenna Design

(a) Antenna Configuration

In this section, we have proposed a novel fractal UWB antenna using Minkowski like fractal geometry. Fractal antenna design includes many segments with different scale ratios, which are repeated frequently. The fractal dimension (D) and effective length (l) of a curve are defined as [Daotie and Mao, 2012] –

$$D = \frac{\log(N)}{\log(r)} \tag{3.1}$$

$$l = h\left(\frac{N}{r}\right)^n \tag{3.2}$$

where N shows the number of segments the geometry have, r represents the number that each segment is divided on each iteration, h is the initial length of the curve and n shows the number of iterations.

Iterated function system (IFS) is an extremely useful method to generate a wide variety of fractal geometries. IFS use a series of transformations such as scaling, rotation and translation [Werner and Ganguly, 2003]. These transformations are expressed as:

$$W\begin{bmatrix} x \\ y \end{bmatrix} = \begin{bmatrix} \frac{1}{r}\cos\theta & \frac{-1}{s}\sin\theta \\ \frac{1}{r}\sin\theta & \frac{1}{s}\cos\theta \end{bmatrix}\begin{bmatrix} x \\ y \end{bmatrix} + \begin{bmatrix} e \\ f \end{bmatrix} \tag{3.3}$$

where r and s are the scaling factors in x- and y- axis respectively, θ is the rotation angles in x-y plane, e and f are the linear translations in x- and y- axis respectively.

The linear transformation matrices for the given Minkowski like curve as shown in Figure 1(b) are given below:

$$W_0 = \begin{bmatrix} 1/5 & 0 & 0 \\ 0 & 1/5 & 0 \\ 0 & 0 & 1 \end{bmatrix}, \quad W_1 = \begin{bmatrix} 0 & -1/5 & 1/5 \\ 1/5 & 0 & 0 \\ 0 & 0 & 1 \end{bmatrix}, \quad W_2 = \begin{bmatrix} 1/5 & 0 & 1/5 \\ 0 & 1/5 & 1/5 \\ 0 & 0 & 1 \end{bmatrix}$$

$$W_3 = \begin{bmatrix} 0 & -1/5 & 2/5 \\ 1/5 & 0 & 1/5 \\ 0 & 0 & 1 \end{bmatrix}, \quad W_4 = \begin{bmatrix} 1/5 & 0 & 2/5 \\ 0 & 1/5 & 2/5 \\ 0 & 0 & 1 \end{bmatrix}, \quad W_5 = \begin{bmatrix} 0 & 1/5 & 3/5 \\ 1/5 & 0 & 2/5 \\ 0 & 0 & 1 \end{bmatrix}$$

$$W_6 = \begin{bmatrix} 1/5 & 0 & 3/5 \\ 0 & 1/5 & 1/5 \\ 0 & 0 & 1 \end{bmatrix}, \quad W_7 = \begin{bmatrix} 0 & 1/5 & 4/5 \\ -1/5 & 0 & 1/5 \\ 0 & 0 & 1 \end{bmatrix}, \quad W_8 = \begin{bmatrix} 1/5 & 0 & 4/5 \\ 0 & 1/5 & 0 \\ 0 & 0 & 1 \end{bmatrix} \tag{3.4}$$

and iterative functions are obtained by applying the methods of transformation:

$$f = \begin{bmatrix} 0 & 1 \\ 0 & 0 \\ 1 & 1 \end{bmatrix} \tag{3.5}$$

$$\begin{aligned} &xy_0 = w_0 f, \quad xy_1 = w_1 f, \quad xy_2 = w_2 f, \\ &xy_3 = w_3 f, \quad xy_4 = w_4 f, \quad xy_5 = w_5 f, \\ &xy_6 = w_6 f, \quad xy_7 = w_7 f, \quad xy_8 = w_8 f \\ &P = \begin{bmatrix} xy_0 & xy_1 & xy_2 & xy_3 & xy_4 & xy_5 & xy_6 & xy_7 & xy_8 \end{bmatrix} \end{aligned} \tag{3.6}$$

where *P* represents all the co-ordinate points of the fractal geometry. This matrix is further used to generate the co-ordinates of each segment.

The first iteration generates the segment by dividing the initial length in five equal parts, and using that segment the Minkowski like structure is generated, as shown in Figure 3.1. The effective length of the Minkowski like geometry increases at each iteration and is given by Eq. (2), which results like $l = h\left(\frac{9}{5}\right)^n$ for this structure. Hence, for first iteration, the length increases by a factor of 1.8 and the fractal dimension for this structure will be $\log(9)/\log(5) = 1.37$, which is closed to Minkowski fractal dimension D = 1.5 [Falconer, 1990]. An iterative recursive code is developed in MATLAB [Matlab] to generate the Minkowski like structure based on Equation (3.3) and is used to generate a *.vbs (visual basic script) file. This *.vbs file is imported into the Ansys HFSS 13.0 to create the desired structure. This geometry is further used as a basic structure for the design of a wideband antenna.

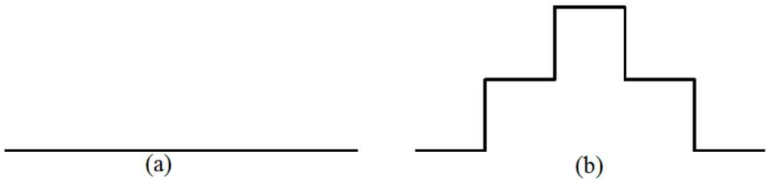

Figure 3.1: Generation of a Minkowski like structure after first iteration using MATLAB (a) Iteration-0 and (b) Iteration-1

The initial design of the antenna is started by combining similar Minkowski like structure segments maintaining the symmetry on a conventional rectangular monopole patch antenna. The addition of the Minkowski like structures increases the effective length of the antenna in order to operate the antenna in UWB range, as shown in Figure 3.2(a). The proposed structure contains many bends and these bends cause the change in the current path, which leads to more and more radiation. Most of the Minkowski like structure segments of the antenna are in the vertical direction. Hence, the overall radiation will be a constructive due to the reinforcement of individual segments in a particular direction. The simulations are carried out on the substrate FR4 of rectangular dimensions (W × L) having dielectric constant of ε_r = 4.4, loss tangent tanδ = 0.02, and thickness h = 1.6 mm. A rectangular substrate is chosen as a basic structure of the proposed antenna due to its characteristic of wideband operability and good radiation property [Tasouji *et al.*, 2013]. The antenna is fed by a 50 Ω microstrip line of width

(W_m). The initial simulation is carried out on rectangular dimensions (23.5 mm × 26.5 mm) with Minkowski like structure's width W_s = 0.5 mm. In order to achieve the desired UWB characteristics and compact size of the antenna, several design parameters of the antenna are optimized. It includes the insertion or the removal of a metallic part from the design. The effect of different design parameters such as Minkowski like structure's width (W_s), ground plane length (L_g) and slots at the ground plane has been investigated.

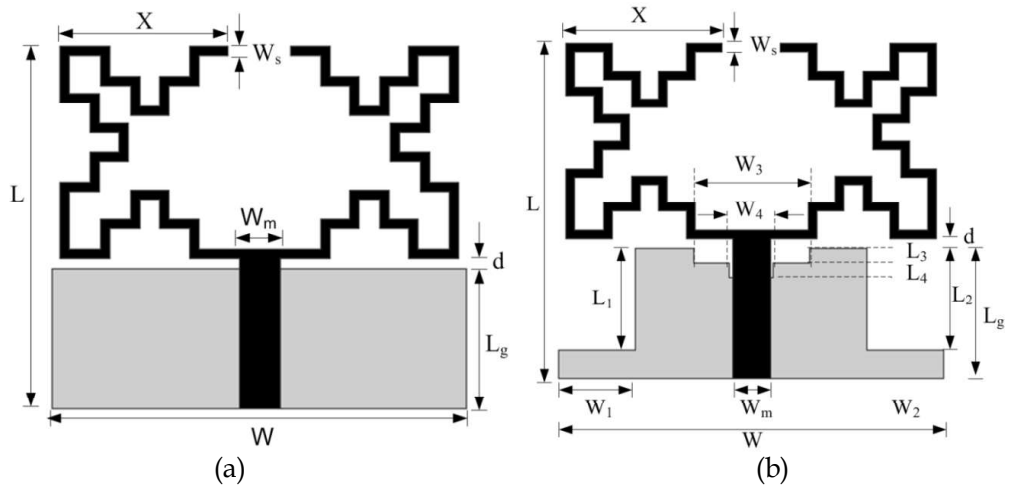

Figure 3.2: Geometrical design of the proposed UWB antenna (a) Initial and (b) Optimized structure

(b) Effect of Minkowski like Structure's Width (W_s)

The proposed fractal antenna is simulated for various values of W_s. It is varied from 0.5 mm to 0.7 mm in steps of 0.1 mm. The simulated S_{11} for different values of W_s is shown in Figure 3.3. As we increase the value of W_s, S_{11} characteristic remains nearly unaltered for the lower frequencies, whereas for higher frequencies S_{11} deteriorates slightly. Hence, W_s = 0.6 mm is chosen as an optimal parameter. These variations in W_s cause the change in the effective area of the fractal antenna, which affects the UWB antenna characteristics.

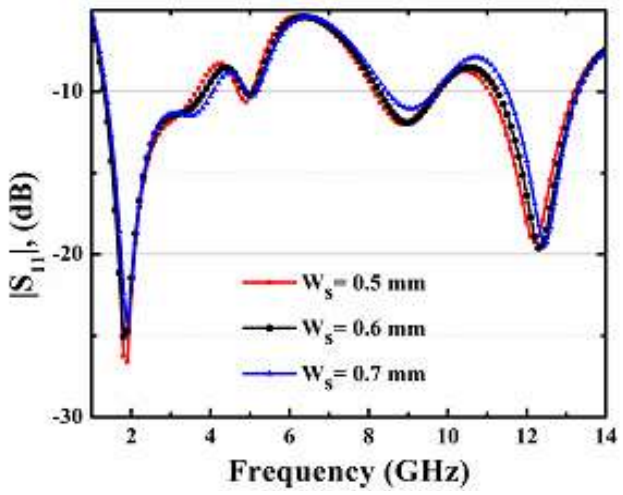

Figure 3.3: Reflection coefficient S_{11} variation for different width of Minkowski like structure strip (W_s)

(c) Effect of Feed Gap (d)

The proposed structure is further simulated for the different feed gap variations (d) between the radiator and the ground plane. This change in feed gap affects the bandwidth significantly because the maximum current density belongs to the circumference of the radiator and the ground plane near to the radiator. The effect of feed gap is analyzed for the optimal W_s = 0.6 mm. The variations in the S_{11} for different feed gaps are shown in Figure 3.4. It can be observed that with the increment in the values of d, $S_{11} \leq$ -10 dB bandwidth deteriorates at higher frequencies of UWB range, whereas it has slight impact on lower UWB operating frequencies. The optimal S_{11} response is obtained for d = 0.7 mm.

(d) Effect of ground plane

The effect of ground length L_g on the S_{11} characteristics is analyzed for the optimal design parameters, W_s = 0.6 mm and d = 0.7 mm, as shown in Figure 3.5. The variation in L_g leads to change in the geometrical area of the ground plane. We perceived that with the increment in the values of L_g, S_{11} varies slightly in the lower frequency edge. However, at higher frequencies in the UWB range S_{11} improves for L_g = 9 mm and again get deteriorated for L_g = 10 mm. Hence, the optimal S_{11} response is selected for L_g = 9 mm.

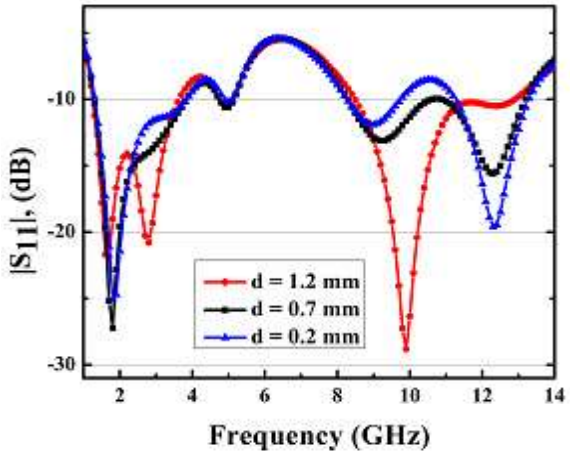

Figure 3.4: Reflection coefficient S_{11} variation for different feed gap thickness (d)

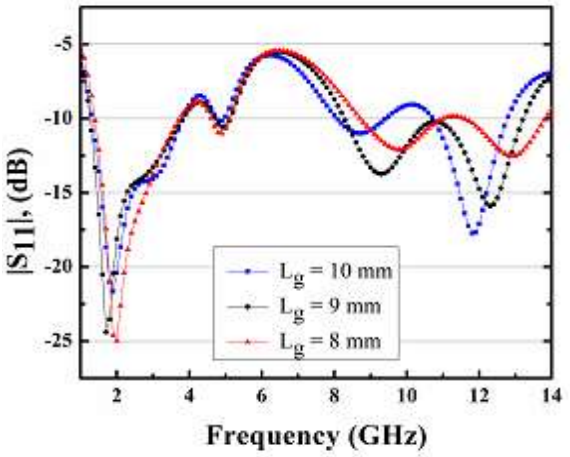

Figure 3.5: Reflection coefficient S_{11} variation for different ground length (L_g)

(e) Effect of Slots at Ground Plane

To further improve the performance of proposed Minkowski like fractal antenna (MLFA), the effect of slots are investigated in the ground plane for optimal values of W_s = 0.6 mm, d = 0.7 mm and L_g = 9 mm. These changes in ground plane leads to the variation in the current path length as well as the area of the ground plane. By introducing slots in the ground plane the effective area of the ground plane changes, which leads to changes in the impedance and bandwidth of the antenna [Tasouji *et al.*, 2013]. The effect of introducing different slots in the ground plane is summarized as below:

(1) MLFA + Slot 1 + Slot 2

By cutting the first ($L_1 \times W_1$) and second ($L_2 \times W_2$) slots at the outer edges of the ground plane lead to an additional resonant frequency at 5.4 GHz. The MLFA antenna with slots shows better results when the dimensions of both slots are equal and symmetric. We have carried out several iterations and the optimal dimensions of slot are selected (7mm × 5.3mm), which covers the entire UWB range. It is observed that the operational bandwidth is obtained between 1.4 – 13.3 GHz as shown in Figure 3.6.

(2) MLFA + Slot 1 + Slot 2 + Slot 3

Considering the fabrication tolerances the obtained results needs to be improved further. Hence, the third slot ($L_3 \times W_3$) is inserted symmetrically across the axis in the ground plane. It disperses surface current distribution and causes to improve S_{11} in the desired UWB frequency range. It is observed that S_{11} improves significantly at higher resonant frequencies as shown in Figure 3.6.

(3) MLFA + Slot 1 + Slot 2 + Slot 3 + Slot 4

Further, the fourth slot ($L_4 \times W_4$) in the ground plane is introduced to accomplish the current distribution in such a manner that it improves S_{11} at higher UWB operational bandwidth edges. The fourth slot shows the improvement in S_{11} characteristics at the middle frequency band and decrement in the higher operating frequency edge as shown in Figure 3.6. Hence, the introduction of the multiple slots in the ground plane leads to the improvement in the bandwidth and S_{11} characteristics of the proposed UWB antenna. The optimized structure of UWB antenna is shown in Figure 2(b). The proposed antenna has an advantage of compact size and simple structure which makes it a better choice for wireless applications. The optimal design parameters of proposed UWB antenna are as follows: L = 23.5 mm, W = 26.5 mm, h = 1.6 mm, X = 10.8 mm, W_m = 2.6 mm, W_s = 0.6 mm, d = 0.7 mm, L_g = 9 mm, L_1 = 7 mm, W_1 = 5.3 mm, L_2 = 7 mm, W_2 = 5.3 mm, L_3 = 1 mm, W_3 = 8 mm, L_4 = 1 mm and W_4 = 3 mm.

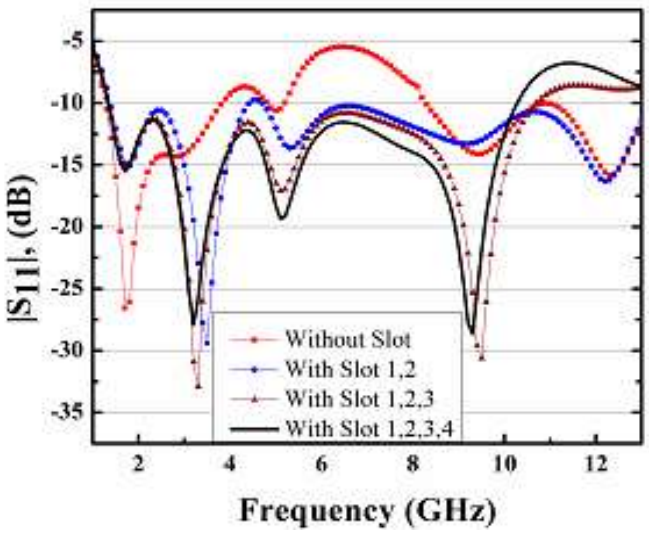

Figure 3.6: Reflection coefficient S_{11} variation with frequency (with and without slots)

The surface current distribution of the proposed antenna along with the ground plane is shown in Figure 3.7, to provide more insight into behavior of the antenna. At low resonant frequencies, the surface current is more intense near the edges of slots, feed line and the initial segments of the radiator, which leads to good impedance matching. At high resonant frequency, the current is distributed more strongly on the feed strip and the edges of the slots and fractal antenna. It is due to the change in the nature of the current and this leads to decrement in the intensity of the current distribution, which causes for the change in impedance matching, gain, and radiation behavior of the antenna [Ahmad, 2011]. The strong surface current is observed at the edges of slot 3, 4 at resonant frequency 5.0 GHz and 9.2 GHz, which indicates a good S_{11} characteristic at these frequencies. Hence, the shape and dimensions of slots should be chosen very carefully because it causes for the change in the electric path length and affects the radiation behavior of the antenna.

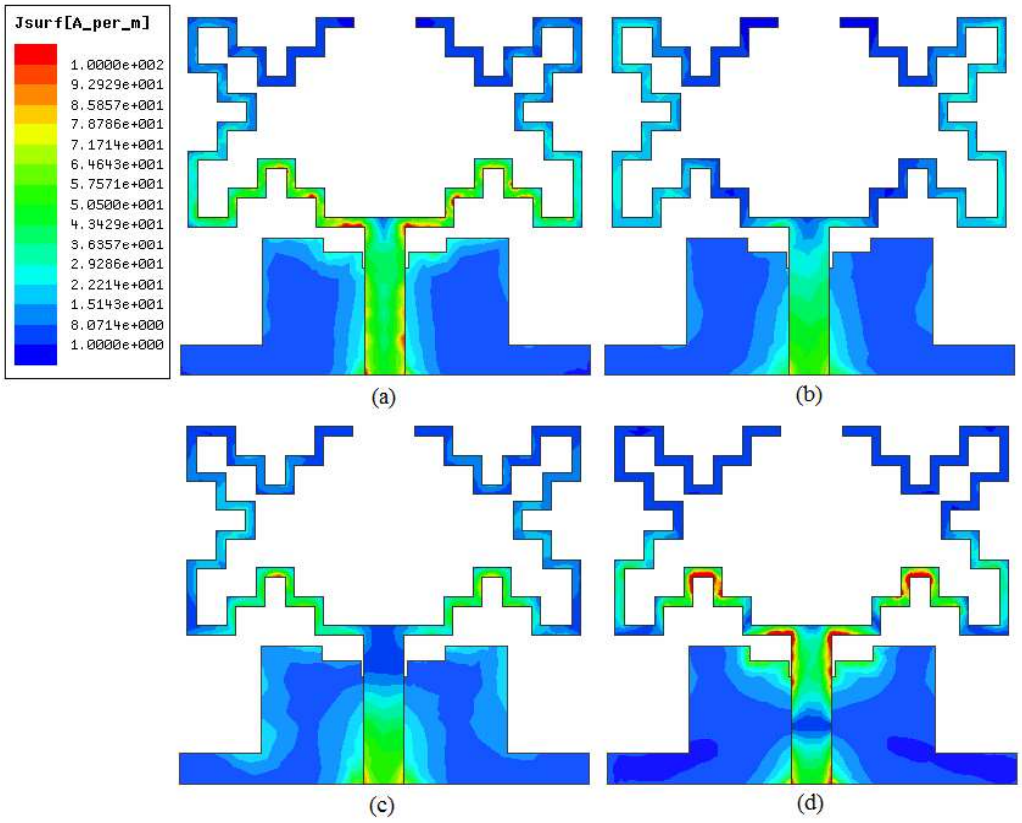

Figure 3.7: Simulated surface current distribution in geometry at resonant frequency (a) 1.7 GHz, (b) 3.2 GHz, (c) 5.0 GHz, and (d) 9.2 GHz

3.2.2 Results and Discussion

(a) S-parameter Result

The optimized geometry of the proposed Minkowski like fractal UWB antenna is fabricated and tested using Agilent vector network analyzer (VNA). Figure 3.8 shows the top and bottom view of the fabricated antenna. The experimental and simulated S_{11} of the antenna is presented in Figure 3.9. It suggests that proposed antenna operates with four distinct resonant frequencies 1.7 GHz, 3.2 GHz, 5.0 GHz, and 9.2 GHz. These results show a promising wide operating bandwidth from 1.4 GHz to 10.4 GHz, covering the entire UWB frequency

range. The experimental result exhibits wideband phenomena from 1.7 GHz to 11 GHz onwards with multiple prominent resonant frequencies in the entire UWB range. The measured result also shows the multiple resonant frequencies, which demonstrates the fractal nature of the Minkowski like structure of the proposed antenna. The experimental result shows good agreement with the simulated one. Some variations are observed due to the measuring environment, fabrication tolerances and losses due to SMA connector. This difference in result may also be caused because of the soldering effect of SMA connector, which is not considered in the simulation.

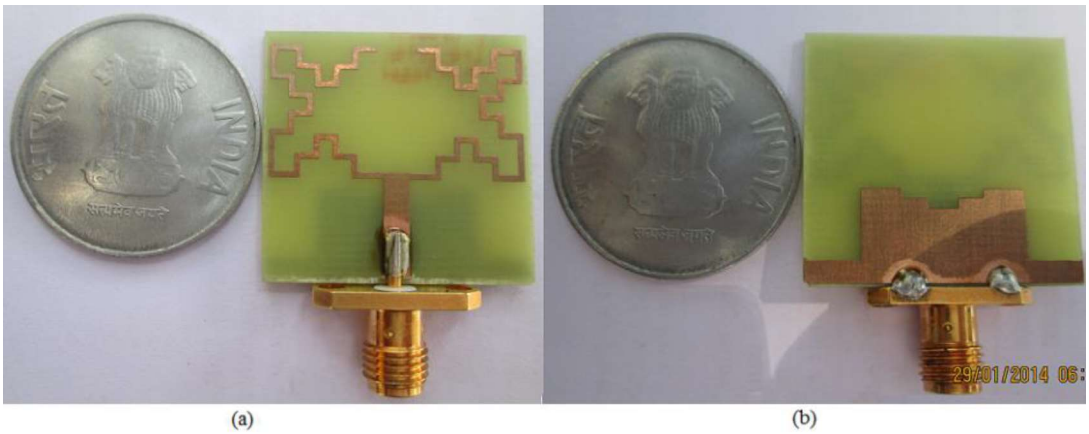

Figure 3.8: Photograph of the fabricated antenna (a) Front view (b) Bottom view

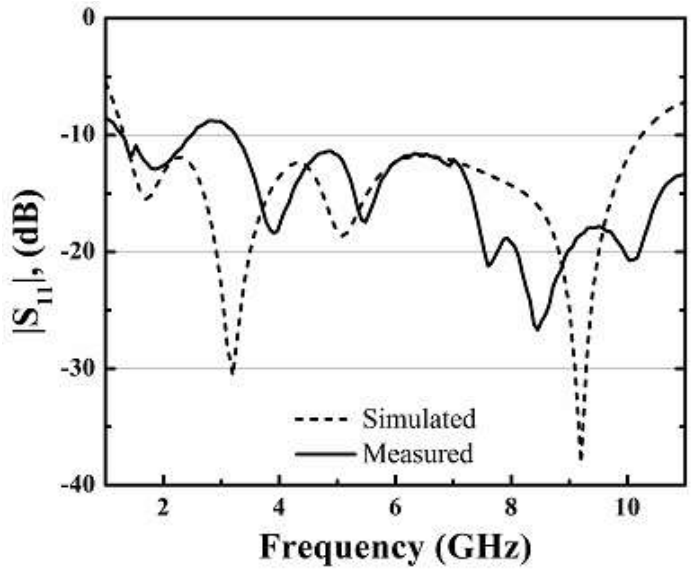

Figure 3.9: Measured and simulated reflection coefficient of antenna with various frequency

(b) Input Impedance Performance

The simulated real and imaginary impedances of the antenna are shown in Figure 3.10. The impedance matching is good at the lower frequency edge as compared to the higher

frequency edge due to the $S_{11} \geq -10$ dB in the high frequency band above 10 GHz as indicated in Figure 3.6. The input impedance of the proposed antenna approaches to 50 Ω at resonant frequencies. The input reactance ranges between -20 to 30 Ω in the UWB range. This indicates the broadband nature of the antenna. The positive and negative part of reactance shows the inductive and capacitive nature of the structure. The variation of the impedance in the UWB range is not too large; this shows the good input impedance matching. Hence, the maximum portion of the power fed to the antenna will be radiated.

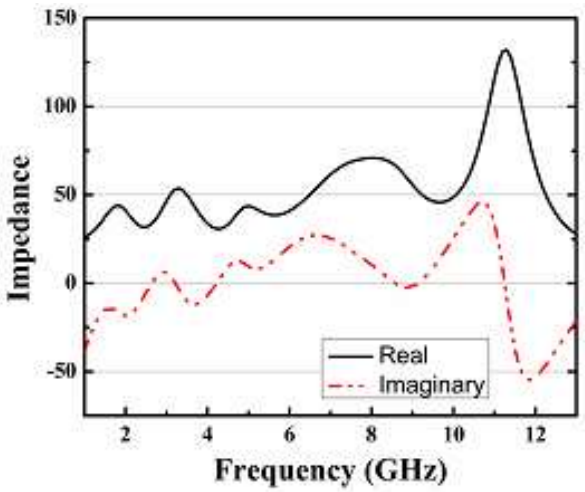

Figure 3.10: Simulated Input Impedance of antenna with variation in frequency

(c) Radiation Performance

Radiation pattern for an antenna is defined mathematically as a function of space co-ordinates (r, θ, φ). The performance of the proposed UWB antenna in the far field region is described using principal *E*-plane (*yz*-plane) and *H*-plane (x*z*-plane) patterns for constant radial distance and frequency [Balanis, 2005]. The radiation patterns have been investigated for optimized Minkowski like structure UWB antenna in the E-planes and H-planes at different resonant frequencies 1.7 GHz, 3.2 GHz, 5 GHz, and 9.2 GHz as shown in Figure 3.11. The radiation patterns are found to be omnidirectional in H-plane and bidirectional in E-plane, but not symmetric across the axis. The cross-pol in H- plane is below -34 dB at all the resonant frequencies. The radiation pattern at higher resonant frequency is distorted compared to the lower ones. It is due to the edge reflection in the fractal antenna and the change in the nature of current from standing wave at lower frequencies to a travelling wave at higher frequencies [Allen *et al.*, 2007]. The gain of the proposed antenna is shown in Figure 3.12. It is observed that gain increases with the increment in frequency at lower UWB operating range.

(d) Time-domain Analysis

The time-domain examination is necessary for the antenna system, which processes short pulses of large bandwidth. Time-domain analysis in terms of fidelity factor is performed to measure the distortion in the input pulse at the time of radiation. The default Gaussian signal covering the UWB range 3.1 GHz to 10.6 GHz, generated in CST Microwave Studio, taken as input signal. This signal satisfies the FCC indoor and outdoor criteria, too. The fidelity factor is calculated by using the method in [Wu *et al.*, 2007]. Table 3.1 presents the value of fidelity factor and it is greater than 0.86. Thus, it can be concluded that the presented antenna structure has a good pulse preserving capability.

Table 3.1: Fidelity Factor of the Presented Antenna

x-*z* plane, θ (°)	0	30	60	90
Fidelity Factor	0.8346	0.8476	0.8631	0.8921

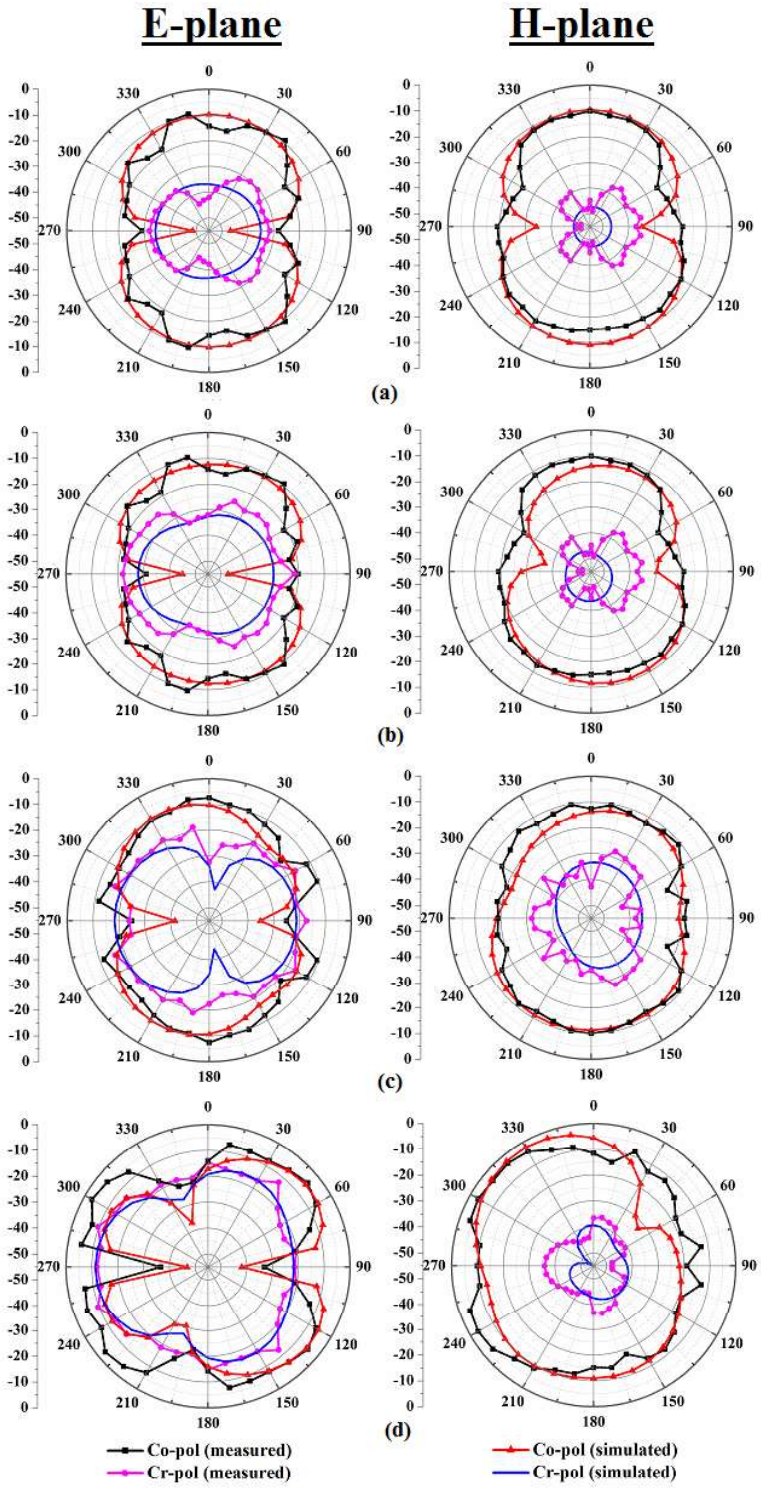

Figure 3.11: Measured and simulated radiation patterns E-planes (x-y plane) and H-planes (y-z plane) at resonant frequencies (a) 1.7 GHz, (b) 3.2 GHz, (c) 5 GHz and (d) 9.2 GHz

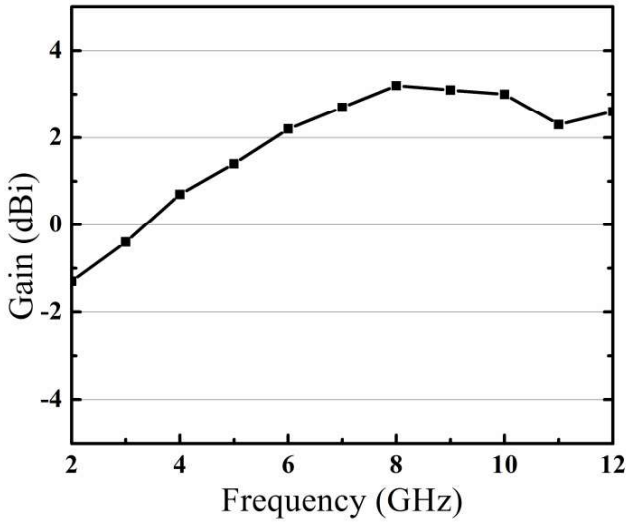

Figure 3.12: Measured gain of the proposed antenna

3.3 Hexagonal Shaped UWB Antenna Using Minkowski Like Fractal Geometry

3.3.1 Antenna Design

In this section, to achieve the miniaturization and wideband phenomena, fractal UWB antenna with rectangular slot in the ground plane is presented. The proposed antenna is generated using Minkowski like fractal and a rectangular slot in the ground plane as shown in Figure 3.13. The substrate Rogers RT/Duroid 5880 having dielectric constant (ε_r) of 2.2, loss tangent (tanδ) of 0.0009 with thickness of 0.787 mm is used for antenna design. The simulations of the initial hexagonal fractal antenna are carried out on a rectangular substrate ($W_{sub} \times L_{sub}$). In the design process basic substrate structure is selected as a rectangular, because rectangular substrate offers wide operational bandwidth and good radiation characteristics [Tasouji *et al.*, 2013]. The proposed antenna is fed by a 50Ω microstrip line (W_{ms}) for impedance matching. To obtain the wideband impedance bandwidth, ground plane is positioned at a distance (d) from the patch, because the current density exists more on the circumference of the hexagonal monopole and the ground near to it. The separation between them affects the impedance matching and return loss characteristics significantly. The optimised dimensions of the proposed fractal UWB antenna are shown in Table 3.2.

The proposed antenna is generated by applying Minkowski like fractal geometry, as shown in Figure 3.1 generated using Eq.(3.3)-(3.6), at the edges of hexagonal shaped monopole. In the design, hexagonal structure acts as an initiator and Minkowski like structure as a generator in the development of initial antenna design, as shown in Figure 3.14.

Table 3.2: Optimized Geometrical Parameters of the Proposed UWB Antenna

Parameters	Dimensions (mm)	Parameters	Dimensions (mm)
L_{sub}	19	L_1	0.2
W_{sub}	15	L_g	3.4
R	4.0	L_s	1.4
W_{ms}	1.65	W_s	3.9
W_{s1}	6.1	D	1.0

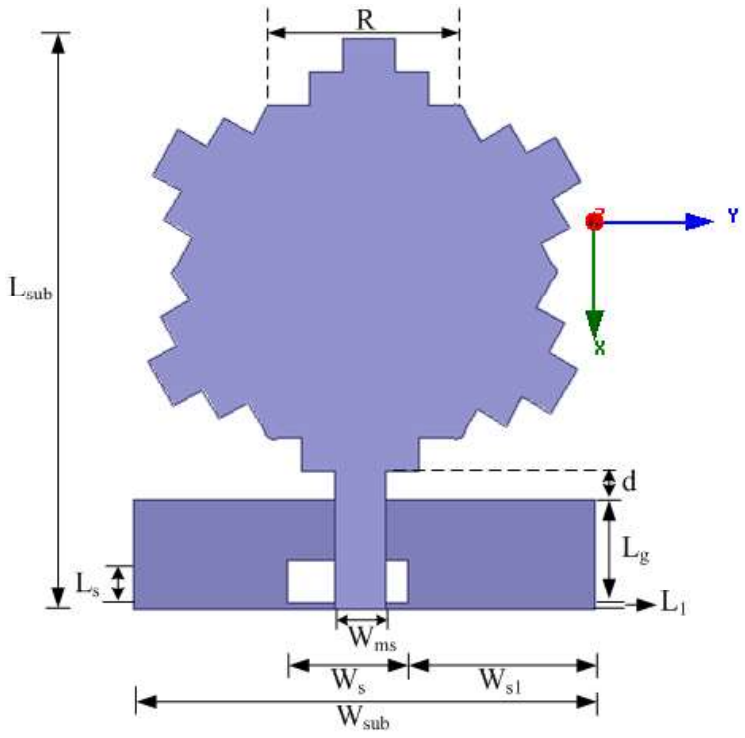

Figure 3.13: Geometry of the optimized hexagonal fractal antenna

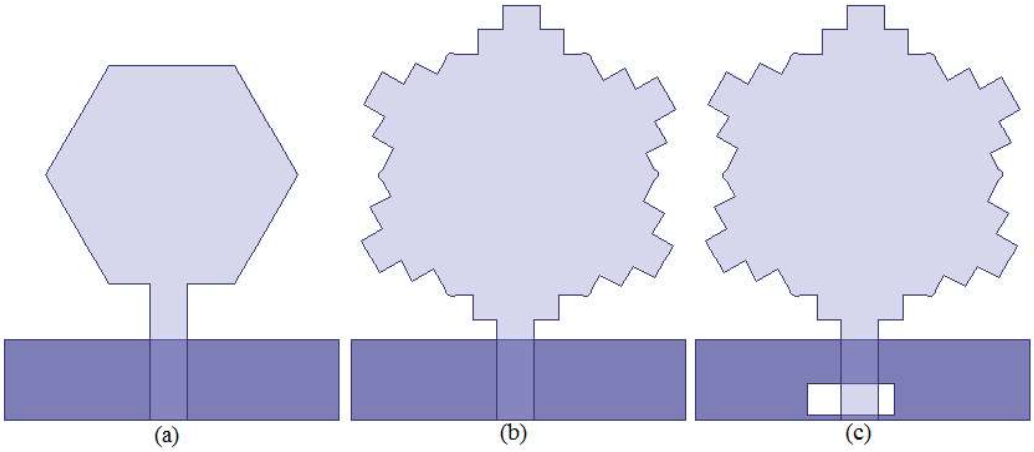

Figure 3.14: Evolution of the proposed antenna (a) antenna without fractal geometry, (b) antenna with fractal geometry and (c) antenna with fractal geometry and rectangular slot

The simulated return loss behaviour of the different antenna generated in the evolution process is shown in Figure 3.15. The application of fractal geometry improves the return loss response in UWB operating range. The multiple resonances contributed by the fractal geometry leads to additional operating bandwidth in the higher frequencies. It is observed that the lower as well as higher frequency band edges are affected after applying rectangular slot in the ground plane. This slot provides shunt capacitance to the feed line which offers another degree of freedom for tuning of input impedance of the antenna. The introduction of slot in the ground changes the effective electrical path length as well as electromagnetic coupling between the

ground plane and the antenna. Moreover, position of slot near to feed line affects significantly the distribution of current intensity, which in turn leads to generation of additional resonant frequency in the higher UWB spectrum as well as offer improvement in the S_{11} characteristics of the antenna in the UWB band. These modifications in the geometry provide a wider operational bandwidth and help to achieve the desired UWB characteristics. In the design process slot is placed asymmetrically near to feed line in order to achieve desired UWB band accurately. However, symmetrical placing of slot in the design did not offer desired results in the UWB band. The proposed antenna is suitable for the entire UWB frequency range with two distinct resonant frequencies at 4.5 and 10 GHz. These simulated results show $S_{11} \leq -10$ dB from 3.1-11.6 GHz, which covers the entire UWB spectrum.

For a regular hexagonal geometry of side length R, area (A_i) and the outer perimeter (L_i), are evaluated in (3.7) and (3.8).

$$A_i = 2.598R^2 = 2.598 \times (5.66)^2 = 83.23 \text{ mm}^2 \tag{3.7}$$

$$L_i = 6R = 6 \times 5.66 = 33.96 \text{ mm} \tag{3.8}$$

The application of Minkowski like structure at the edges of hexagonal geometry will increase the final effective area (A_f) as well as final effective outer perimeter (L_f). A_f and L_f are calculated as-

$A_f = A_i + 6 \times$ Area increased by a single Minkowski like structure = 113.98 mm^2

$$L_f = 6\left(\frac{9}{5}\right)^1 \times R = 61.08 \text{ mm}$$

The area of hexagonal structure required corresponding to perimeter of 61.08 mm will be 269.66 mm^2. Hence, the application of Minkowski like fractal geometry helps to achieve the same perimeter by a significant reduction of 57.73% in area.

The current distribution pattern of the proposed UWB antenna at resonant frequencies 4.5 GHz and 10 GHz is shown in Figure 3.16. At 4.5 GHz, the current density is mainly distributed along the feed line, the lower edge of the monopole, and the upper as well as middle section of the ground plane. It can be seen that the introduction of slot in the ground plane has a significant effect on the proposed antenna characteristics. The intensity of surface current distribution is more at fractal edges at higher resonant frequency compared to lower resonant frequency [Fereidoony *et al.*, 2012].

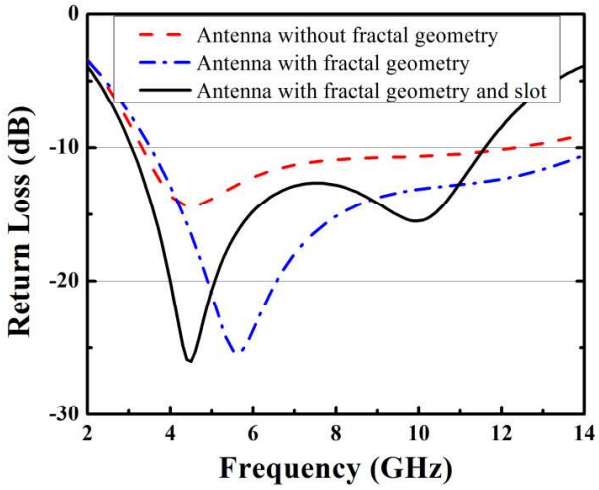

Figure 3.15: Simulated return loss characteristics for different antenna shown in Figure 3.12

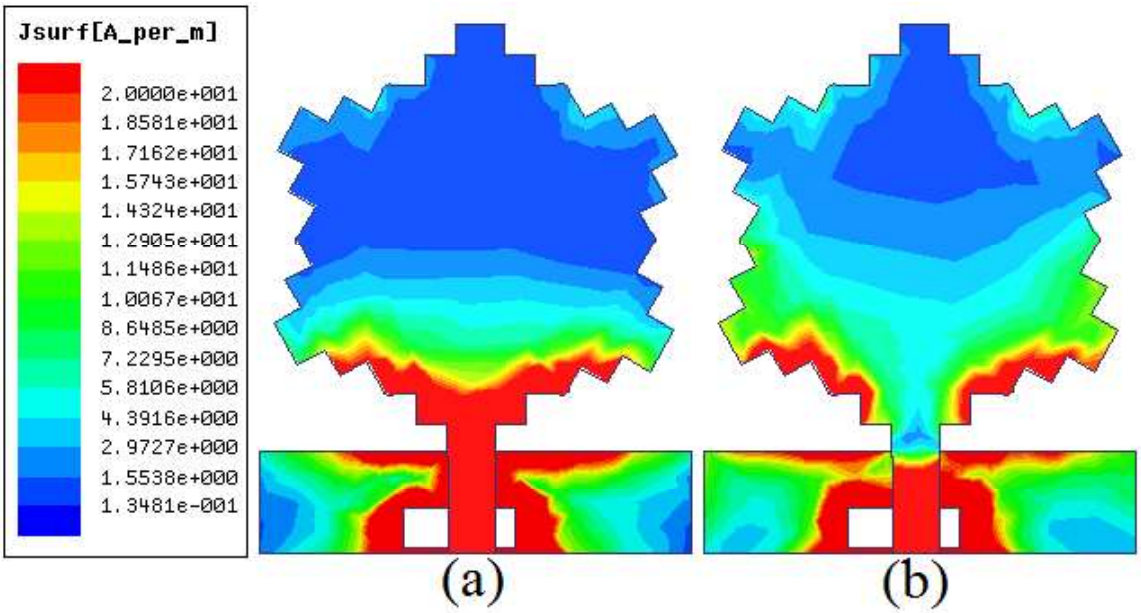

Figure 3.16: Current distribution in geometry at resonant frequency (a) 4.5 GHz, and (b) 10 GHz

3.3.2 Results and Discussion

(a) S-parameter Result

The optimized hexagonal fractal UWB antenna is fabricated and S_{11} is measured using vector network analyzer (VNA) E5071C. Figure 3.17 shows the top and bottom view of the fabricated prototype of the proposed UWB antenna. The measured and simulated return loss of the antenna is plotted in Figure 3.18, and a good agreement between them is observed. It is observed from measured results that the fabricated antenna exhibits the operational impedance bandwidth from 3.2-14 GHz with two resonant frequencies at 5 GHz and 10.6 GHz. However, some discrepancies are observed due to the measurement environment, SMA connector losses and the fabrication tolerances.

Figure 3.17: Photograph of the fabricated antenna (a) Front view (b) Bottom view

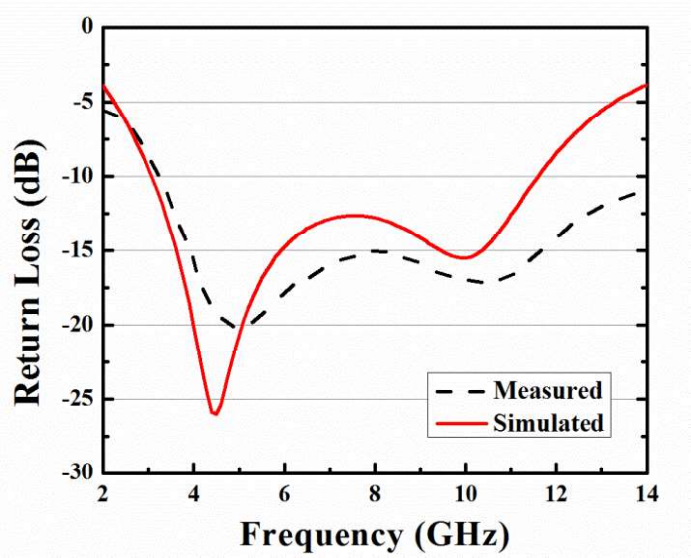

Figure 3.18: Comparison of the simulated and measured return loss characteristics of the antenna

(b) Input Impedance Performance

The simulated real and imaginary impedance of the antenna is shown in Figure 3.19. The impedance matching is good at the lower frequencies as compared to the higher frequencies. The input reactance ranges between -30 to 30 Ω in the UWB range. This indicates the broadband nature of the antenna. It can be seen that the flat response of both the real and imaginary part of the input impedance resulting in a broadband bandwidth from 3.1 GHz to 11.6 GHz. The variations in the impedance over the UWB operating ranges are in acceptable range. The real input impedance of the proposed antenna approaches to 50 Ω at resonant frequencies. This low input impedance makes this antenna structure suitable for entire UWB frequency band.

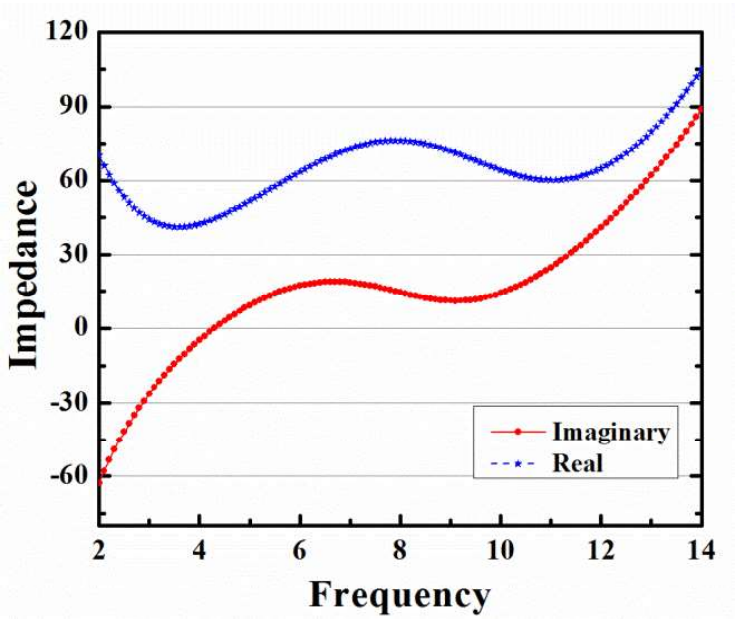

Figure 3.19: Simulated Impedance variation of the proposed antenna with frequency variation

(c) Radiation Performance

The performance of fractal UWB antenna in the far field region is described using its principal *E*-plane (*xz*-plane) and *H*-plane (*yz*-plane) patterns for constant radial distance and frequency, displayed in Figure 3.20. The radiation patterns are found to be omnidirectional in the H-plane and bidirectional shapes in the E-plane with very low cross polarization mostly below -20 dB. The radiation pattern behaviour at higher resonant frequency is also nearly omnidirectional because of the extra current presents at the fractal edges of the Minkowski like structure in the monopole, which leads to stable radiation pattern [Allen *et al.*, 2007]. The measured gain of the presented antenna is shown in Figure 3.21. It is observed that after 5 GHz gain response is steady in the UWB operating range.

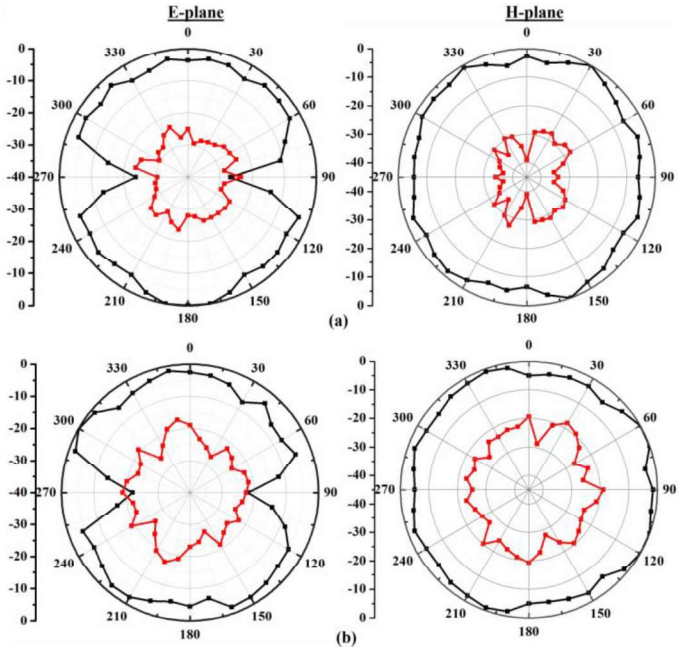

Figure 3.20: Measured radiation patterns with co polarization (—) and cross polarization (—) for H-planes and E-planes at (a) 4.5 GHz, and (b) 10 GHz

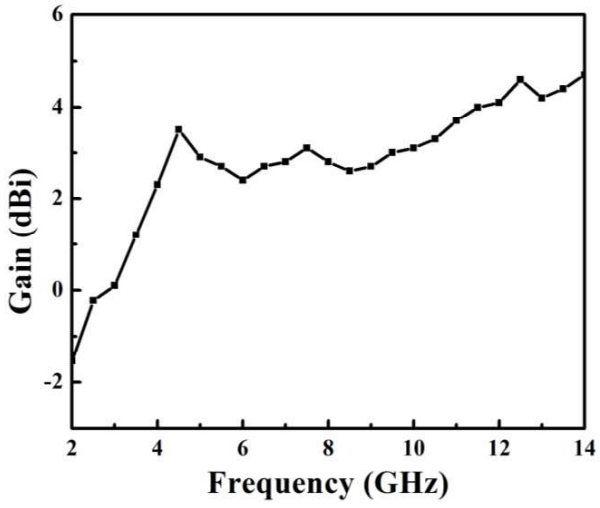

Figure 3.21: Measured gain of the proposed fractal UWB antenna

(d) Time-domain Analysis

The time-domain analysis of is necessary for wideband antenna system. Hence, the time domain analysis in terms of fidelity factor is performed to evaluate the distortion in the input pulse at the time of radiation. The fidelity factor is calculated by using the method in [Wu *et al.*, 2007]. Table 3.3 shows the value of fidelity factor and it is greater than 0.82. It demonstrates that the radiated waveform is little distorted as compared with the excited signal.

Table 3.3: Fidelity Factor of the Presented Antenna

x-z plane, θ (°)	0	30	60	90
Fidelity Factor	0.8872	0.8216	0.8592	0.8931

3.4 Octagonal Shaped UWB Antenna Using Minkowski Like Fractal Geometry

3.4.1 Antenna Design

In this section, we have presented a small novel fractal UWB antenna with slotted ground plane. The iteration wise application of Minkowski like fractal geometry at the edges of octagonal geometry is shown in Figure 3.22. In the development of initial antenna design, this octagonal shape works as an initiator and Minkowski like fractal shape works as a generator. The proposed antenna based on a combination of the Minkowski like fractal and octagonal geometry, generated using Eq. (3.3)-(3.6), is shown in Figure 3.23.

The proposed antenna is examined and designed by simulation software program Ansoft HFSS v.13, based on a three-dimensional (3D) full-wave finite element (FE) method. The proposed antenna design is simulated on a rectangular substrate (W×L), Rogers RT/Duroid 5880, having a dielectric constant of ε_r = 2.2, loss tangent tanδ = 0.0009, and thickness of 0.787 mm. The basic shape of the substrate for the antenna design is chosen as a rectangular. The selection of rectangular substrate offers wideband operability and good radiation property [Tasouji *et al.*, 2013]. The patch is connected to a 50 Ω micro strip line of width (W_m) and length (L_m) for impedance matching. Ground plane is positioned on the other side of the substrate of length (L_g) and width (W). To achieve the desired characteristic and compact size of the proposed octagonal fractal antenna (OFA), an optimization of the different bandwidth enhancement design parameters has been carried out. Thus, the feed gap (d) between the radiator and the ground plane near to radiator, the length and width of radiator and width (W) of the ground plane have been adjusted to obtain the desired characteristics.

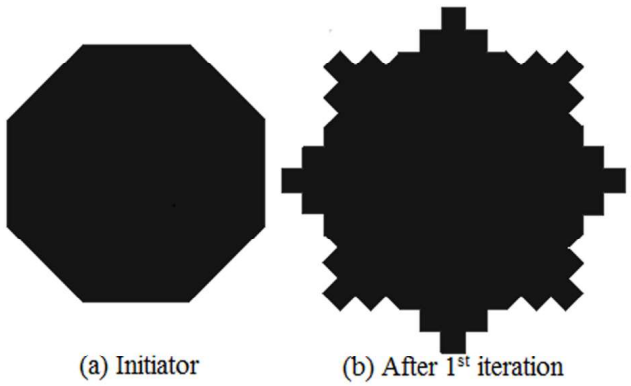

Figure 3.22: Minkowski like fractal as applied to the edges of Octagonal geometry

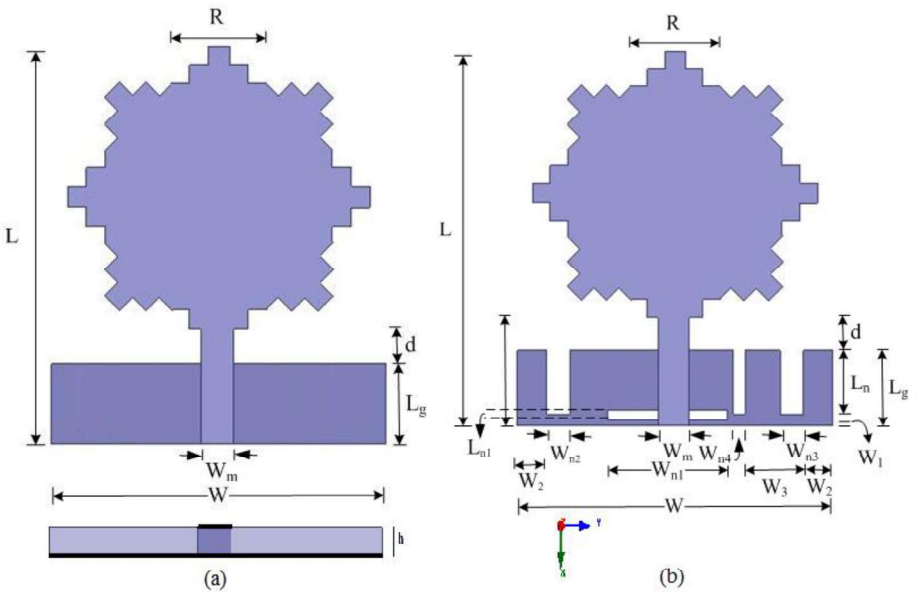

Figure 3.23: Geometry of the proposed Octagonal fractal antenna (a) Initial (b) Optimized structure

The variation in above parameters affects the impedance matching and return loss characteristics, because the surface current density exist more on the circumference of radiator and the ground near to radiator. After the optimization of these parameters, the initial OFA antenna as shown in Figure 2(a) is obtained. It shows return loss characteristic from 3.6 GHz onwards with a resonant frequency at 5.2 GHz as shown in Figure 3.24. Hence, in order to obtain the desired UWB bandwidth perturbation in the ground plane is introduced, which leads to the changes in the current path. These changes in the ground plane of the antenna are responsible for the modifications in the current path length, which implies changes in the impedance and bandwidth of the antenna [Tasouji *et al.*, 2013]. The effect of introducing different notches in ground plane is summarized as below:

(a) OFA + Notch 1

By cutting the first notch ($L_{n1}\times W_{n1}$) near the excitation in the ground plane leads to an additional resonant frequency at 10.6 GHz. It is observed that the operational bandwidth is obtained between 3.2-12 GHz, which does not cover the desired UWB bandwidth. As we increases the width (W_{n1}) of the notch operating frequency range of lower frequency band shifted towards right slightly, whereas higher frequency range shows a significant change with improved return loss characteristic. Increasing the length of notch 1 (L_{n1}) towards left side causes for the degradation in S_{11} in the higher frequency operating range, whereas right side increment shows enhancement in return loss result at lower frequency with reduction in operating range from higher frequency side.

(b) OFA + Notch 1 + Notch 2 + Notch 3

The insertion of second ($L_n\times W_{n2}$) and third ($L_n\times W_{n3}$) notches symmetrically on the both the edges of the ground plane, disperses surface current distribution and causes new path to obtain the desired frequency band from 3.1-10.9 GHz. It is observed that two resonant frequencies at 4.3 and 9.7 GHz are present in the UWB operating range as shown in Figure 3.

(c) OFA + Notch 1 + Notch 2 + Notch 3 + Notch 4

Further, the fourth notch ($L_n\times W_{n4}$) in the ground plane is introduced to accomplish the current distribution in such a manner that it achieves UWB operational bandwidth precisely from 3.1-10.6 GHz. It shows the improvement in return loss characteristics at the middle frequency band of UWB range with resonant frequencies at 4.2 and 9.4 GHz as shown in Figure 3. Using this type of design technique many other wideband antennas can be designed in smaller size.

The surface current distribution pattern on the proposed antenna along with the ground plane is shown in Figure 3.25. At low frequency, the surface current is mainly concentrated near the notch structure edges, and the initial part of the patch antenna, which leads to good impedance matching at 4.2 GHz. At high frequency, most of the current is distributed more strongly on the feed strip and the edges of the fractal antenna and notch surroundings. It is due to the change in the nature of the current and this leads to decrement in the intensity of the current distribution, and causes for the changes in impedance matching, gain, and radiation behavior of the antenna [Ahmed, 2011]. This shows that notches affect the antenna performance at lower and higher frequencies. It can be observed that the current density in antenna part is always stronger than the ground plane because of its fractal nature. Thus, the fractal nature of the antenna affects significantly the impedance matching and the radiation property. At the lower frequencies, the wavelength of the EM waves is long and small segments of the Minkowski like structure contribute less in the overall radiations. However, at higher frequencies, the segment dimensions become comparable to the wavelength, which enhance the radiation characteristic significantly [Baliarda *et al.*, 1998]. Thus, considering such geometrical variations, the optimized design parameters of proposed octagonal fractal UWB antenna is listed in Table 3.4.

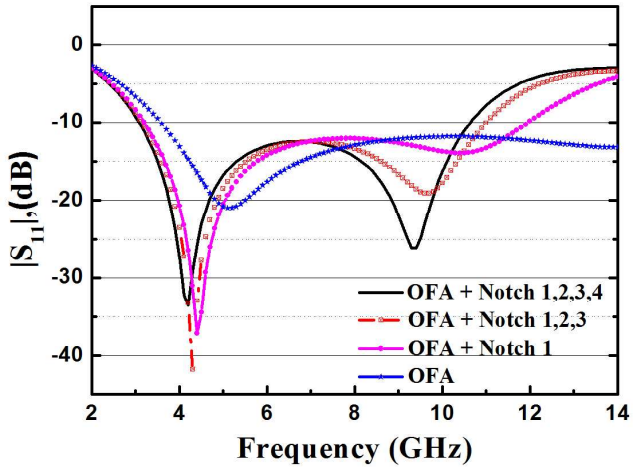

Figure 3.24: Simulated return loss variation with frequency (with and without notch)

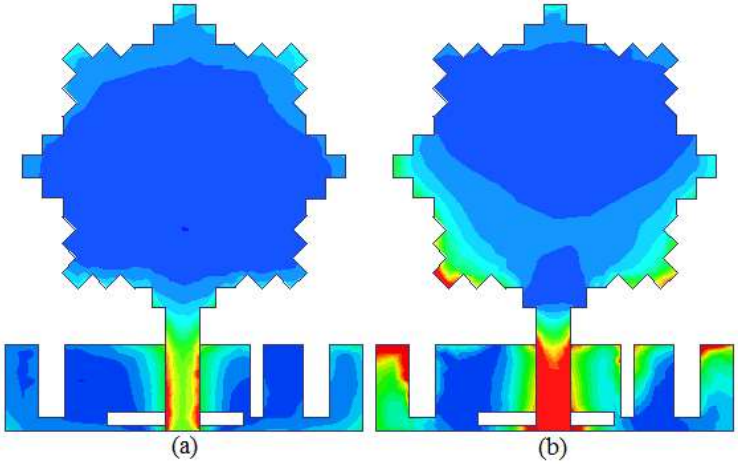

Figure 3.25: Simulated surface current distribution at resonant frequency (a) 4.2 GHz, and (b) 9.4 GHz

Table 3.4: Optimized Geometrical Parameter of the Presented UWB Antenna

Parameters	Dimensions (mm)	Parameters	Dimensions (mm)
L	16.5	W_{n1}	5.15
W	13.5	L_{n1}	0.47
R	3.5	L_n	2.75
W_m	1.32	W_{n2}	1.0
W_1	0.23	W_{n3}	1.0
W_2	1.5	W_{n4}	0.5
W_3	3.8	d	1.4
L_m	4.65	L_g	3.35

3.4.2 Results and Discussion

(a) S-parameter Result

The optimized octagonal fractal UWB antenna is fabricated and tested using Agilent vector network analyzer (VNA). Figure 3.26 shows the fabricated prototype of the top and bottom side of the proposed antenna. The measured and simulated return loss of the UWB antenna is plotted in Figure 3.27, and shows good matching. It is observed that fabricated antenna exhibits the entire UWB frequency range. The experimental results show a little variation at the lower operating frequency around 3 GHz, which implies that the impedance matching of the antenna is less dependent on ground plane [Chen *et al*, 2007]. Some discrepancy is observed due to the measurement environment, losses introduced by SMA connectors and the fabrication tolerances.

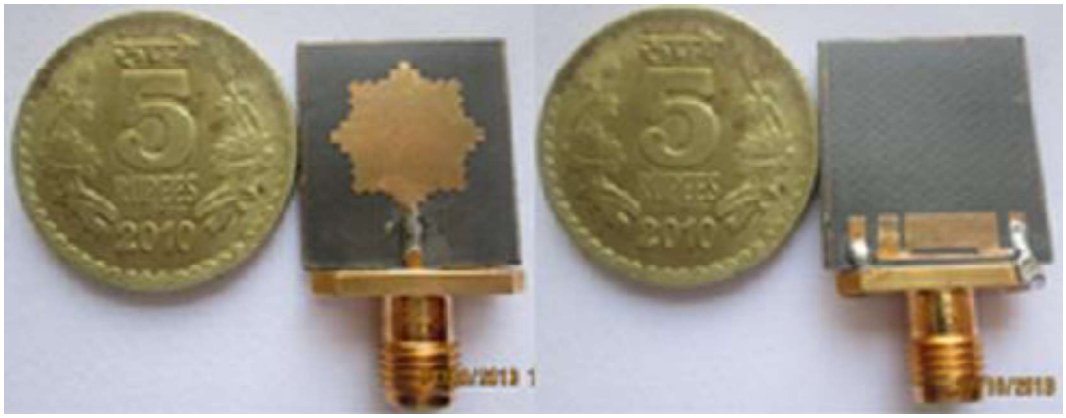

(a) (b)

Figure 3.26: Photograph of the fabricated antenna (a) Front view (b) Bottom view

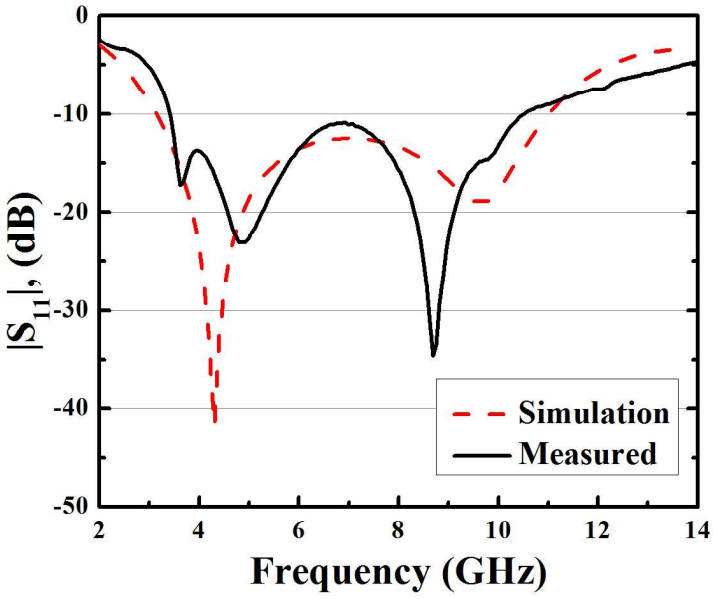

Figure 3.27: Measured and simulated return loss of proposed UWB antenna

(b) Input Impedance Performance

The simulated real and imaginary impedance of the antenna is shown in Figure 3.28. The impedance matching is good at the higher frequency edge as compared to the lower frequency edge. It can be observed from the Figure 3.25; the introduction of notch in the ground plane deteriorates the S_{11} at the lower frequency edge of UWB antenna and simultaneously improves S_{11} at higher frequency band. The input reactance ranges approximately between -45 to 30 Ω in the UWB range. This indicates the broadband nature of the antenna. The real input impedance of the proposed antenna approaches to 50 Ω at resonant frequency 4.2 GHz and 9.4 GHz respectively. The change in the impedance over the operating range shows the acceptable variation, which makes this antenna structure suitable for entire UWB frequency band.

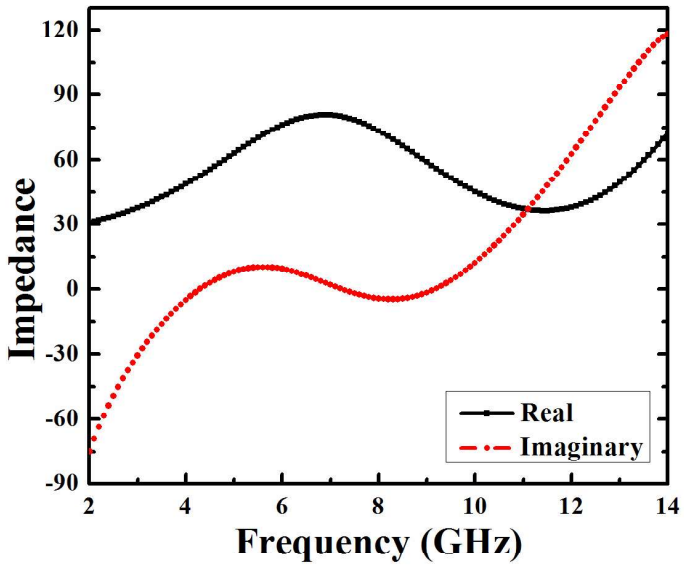

Figure 3.28: Simulated result of real and imaginary impedance

(c) Radiation Performance

Figure 3.29 shows the measured radiation pattern, which deals with the antenna's directional behavior in the far field region using principal *E*-plane (*xz*-plane) and *H*-plane (*yz*-plane) patterns for constant radial distance and frequency [Balanis, 2005]. The radiation patterns are found to be omnidirectional in H-plane and bidirectional in E-plane with low cross-polarization, but not symmetric across the axis at the resonant frequencies of 4.2 GHz, and 9.4 GHz, irrespective of the symmetric structure of the proposed novel antenna. This asymmetry in the radiation patterns existed due to the asymmetrical structure of notches in the ground plane across its axis. The measured result shows a good match with simulated results. However, small deviations in the measured results are observed due to ground plane and edge diffraction. At higher frequencies, the variation is observed in the radiation pattern due to two main reasons. Firstly, due to the reflection at edges from the fractal antenna structure, and secondly, due to the change in the current nature from standing wave pattern at lower frequencies to a travelling wave pattern at higher frequencies [Allen *et al.*, 2007]. This shows good matching and lower reflection at the desired frequency. Figure 3.30 shows the gain of the presented antenna. It is evident from Figure that its gain is low in the lower frequencies due to the smaller dimension of the antenna.

(d) Time-domain Analysis

The time-domain analysis of the wideband antenna system is necessary. The time-domain analysis in terms of fidelity factor is performed by using the method in [Wu *et al.*, 2007]. Fidelity factor measure the distortion in the input pulse at the time of radiation and it is more than 0.84 as shown in Table 3.5. This illustrates that the proposed structure has a good pulse preserving capability.

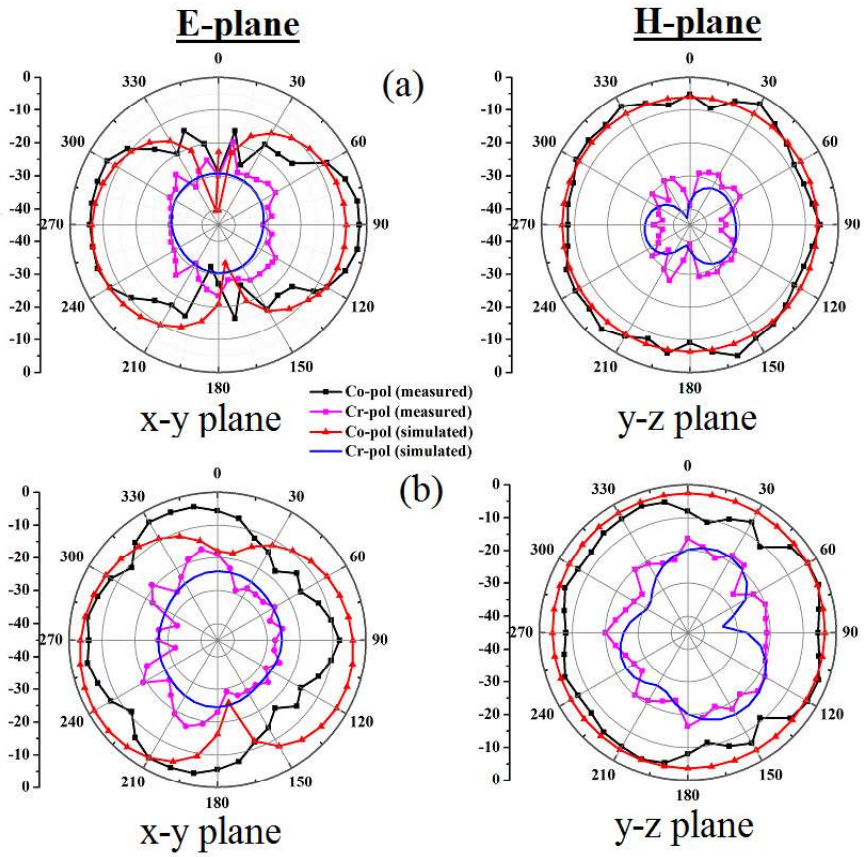

Figure 3.29: Radiation patterns for the proposed fractal UWB antenna with co-polar and cross polar at resonant frequencies (a) 4.2 GHz and (b) 9.4 GHz

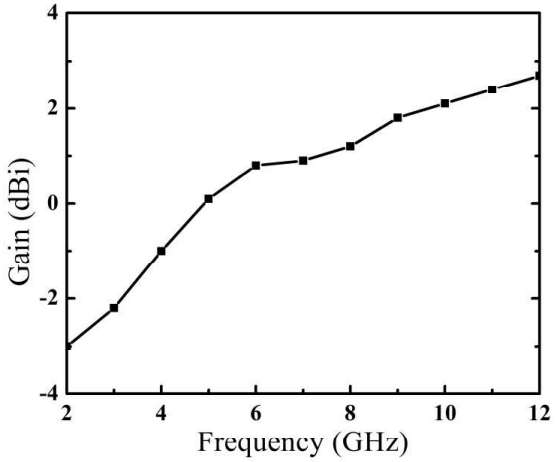

Figure 3.30: Measured gain of the proposed antenna

Table 3.5: Fidelity Factor of the Presented Antenna

x-z plane, θ (°)	0	30	60	90
Fidelity Factor	0.9096	0.8425	0.8774	0.8821

3.5 Octagonal Shaped UWB Antenna Using Minkowski Fractal Geometry with Bandwidth Enhancement

3.5.1 Antenna Design

In this section, we have proposed a small novel UWB antenna based on Minkowski fractal geometry. The Minkowski fractal structure is combined with octagonal shaped geometry to increase the effective length of monopole. Moreover, the application of Minkowski geometry offers miniaturization and wideband phenomena, which helps to achieve 125% fractional bandwidth. In order to obtain the entire UWB frequency range antenna parameters are optimized. The proposed fractal UWB antenna is shown in Figure 3.31. The UWB antenna with and without fractal geometry is simulated using Ansoft HFSS v.13. The proposed antenna design is simulated on a rectangular substrate (W×L), FR4 epoxy, having a dielectric constant (ε_r) 4.4, loss tangent (tanδ) 0.023, and thickness (h) 1.6 mm. The basic structure of the substrate is selected as rectangular because of its wide operating bandwidth and good radiation characteristics [Tasouji *et al.*, 2013]. The monopole is connected to a 50 Ω microstrip line of width (W_m) and length (L_m) for impedance matching as shown in Figure 3.31. The ground plane of length (L_g) and width (W) is placed on the other side of the substrate. The simulations are performed to achieve the optimised dimensions of the proposed antenna as: L = 25.5 mm, W = 16 mm, h = 1.6 mm, R = 4.59 mm, W_m = 2.6 mm, L_m = 11.5 mm, L_g = 10.2 mm.

The proposed antenna is generated by applying Minkowski fractal at the edges of octagonal geometry. The first iteration divides the initial length, as shown in Figure 3.32(a), in three equal parts, and using that segment the Minkowski structure is generated, as shown in Figure 3.32(b). Figure 3.32(c) shows the second iteration of the geometry, which increases the effective length further. Here, in the evolution of antenna design selected octagonal geometry and Minkowski geometry works as an initiator and generator, respectively, as shown in Figure 33. Figure 3.33(a) represents the initial structure without fractal application. Figure 3.33(b) and

3.33(c) shows the antenna structure with the application of first and second iteration of Minkowski fractal geometry at the edges of octagonal geometry, respectively.

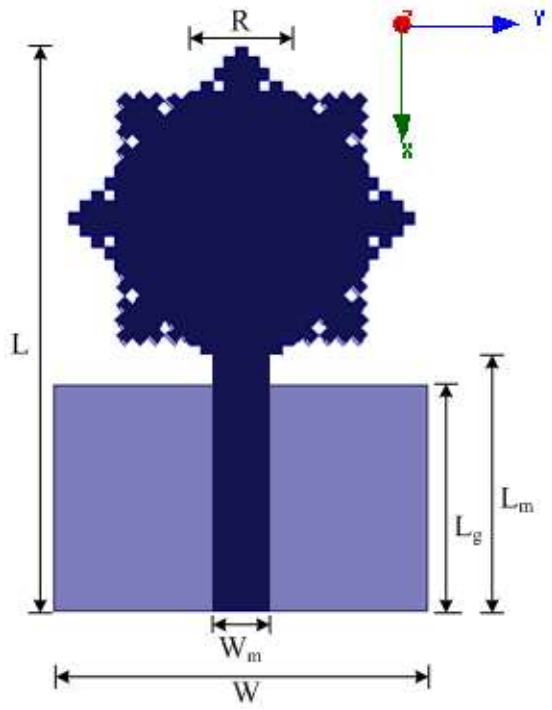

Figure 3.31: Geometry of proposed fractal UWB antenna

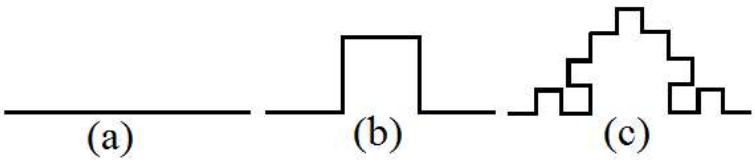

Figure 3.32: Recursive Generation of Minkowski structure (a) Iteration-0 (b) Iteration-1 and (c) Iteration-2

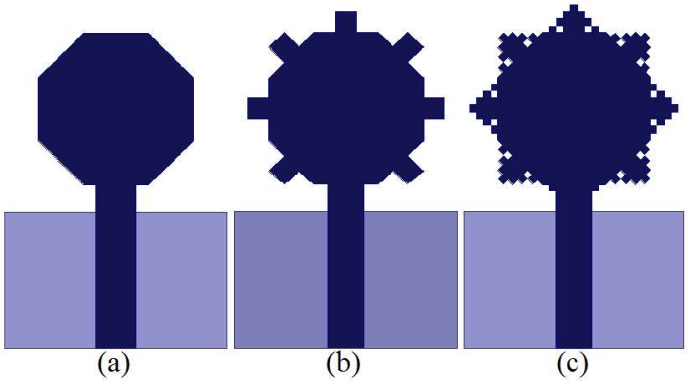

Figure 3.33: Evolution of Antenna structures with the application of Minkowski structure as applied to the edges of Octagonal geometry (a) Antenna-0 (b) Antenna-1 and (c) Antenna-2

The return loss (S_{11}) characteristics of the antenna created in the evolution process are shown in Figure 3.34. The introduction of Minkowski fractal in antenna design excites additional resonance with each iteration as well as improves the return loss behaviour too. The lower operating frequency is also decreases slightly with increase in effective length of the fractal monopole. Moreover, the bends and curves present in the fractal geometry changes the direction of current, which in turn leads to enhancement in the radiation characteristics of the proposed antenna [Balanis, 2005]. The additional generated multiple resonances are combined and leads to wideband phenomena. These modifications in geometry help to achieve the 125% of UWB bandwidth from 2.1 GHz to 12 GHz with three resonant frequencies at 3.4 GHz, 6.5 GHz and 10.5 GHz. The surface current distribution of the antenna is illustrated in Figure 3.35 for better understanding of radiation mechanism. It is observed that current is mainly distributed at near the feed line, ground plane below the feed line and at the edges of the Minkowski fractal geometry. Moreover, the current distribution at the edges of the Minkowski fractal increases at higher frequencies. The fractal edges are responsible for the change in current path, which leads to enhancement in radiation characteristics of the antenna.

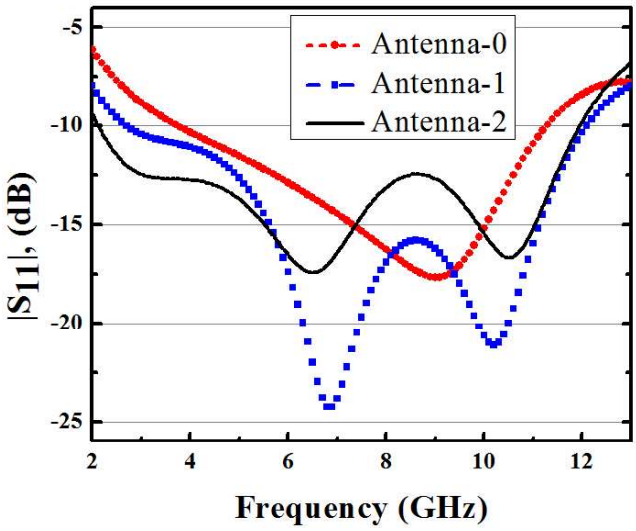

Figure 3.34: Return loss characteristics of the antenna for different antenna structure generated in the evolution process

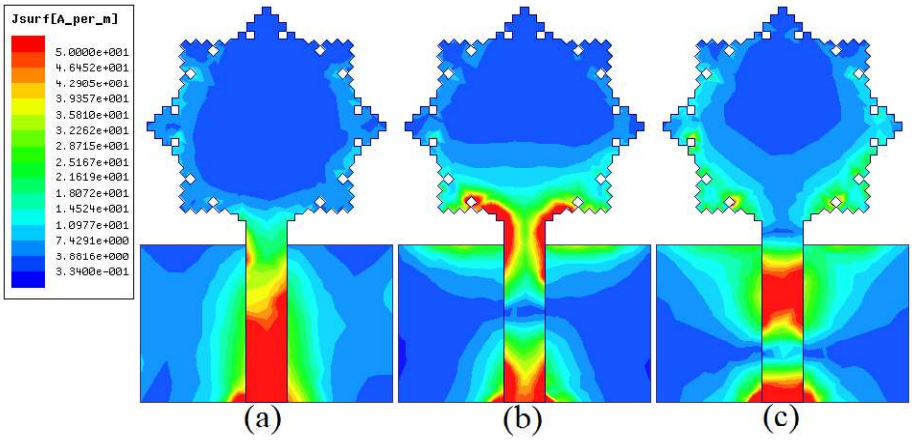

Figure 3.35: Surface current distribution at (a) 3.4 GHz, (b) 6.5 GHz and (c) 10.5 GHz

3.5.2 Results and Discussion

(a) S-parameter Result

The optimized structure of octagonal shaped fractal UWB antenna is fabricated to verify the simulated results. The fabricated prototype of the antenna is shown in Figure 3.36. The return loss is measured by Agilent vector network analyzer (VNA) E5071C. The measured and simulated return loss of the UWB antenna is plotted in Figure 3.37, and shows good matching. It is observed that the entire UWB frequency range is exhibited by the fabricated antenna from 2.9 GHz to 12.5 GHz with multiple resonant frequencies. Moreover, some discrepancies are observed in the result due to the measurement environment, losses introduced by SMA connectors and the fabrication tolerances.

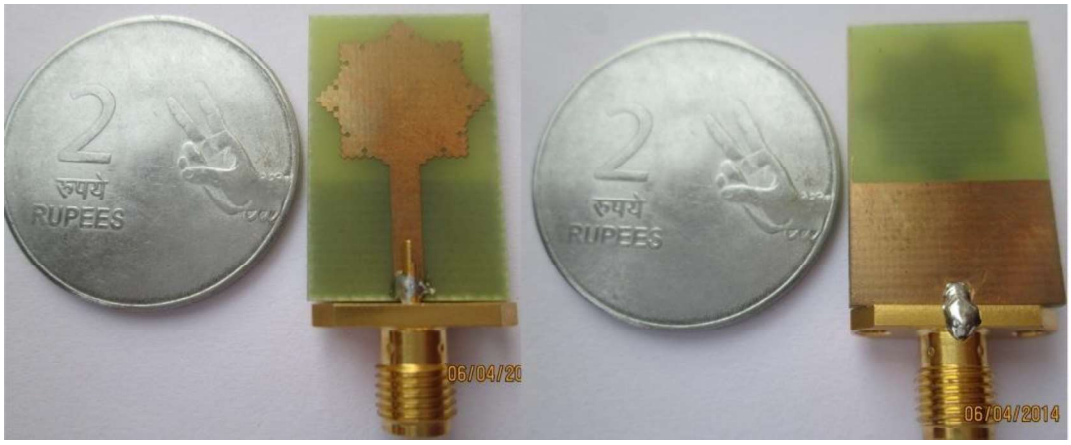

Figure 3.36: Fabricated prototype of the proposed antenna

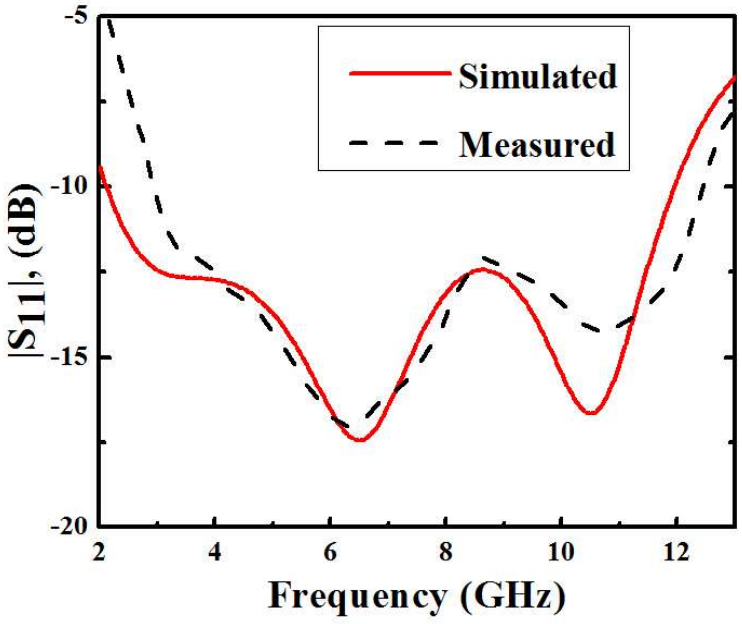

Figure 3.37: Measured and simulated return loss of antenna with various frequencies

(b) Radiation Performance

The radiation patterns are found to be omnidirectional in the H-plane (yz-plane) and bidirectional in the E-plane (xz-plane) at different resonant frequencies as shown in Figure 3.38. The radiation pattern behaviour at higher resonant frequency is also nearly omnidirectional because of the extra current presents at the fractal edges of the Minkowski structure in the monopole, which leads to stable radiation pattern [Fereidoony *et al.*, 2012]. The cross polarization at low resonant frequency is below -15dB. It increases with the increase of frequency, but still below -10 dB level. This shows good matching and lower reflection at the desired frequency. The measured gain of the proposed antenna in the UWB operating range is shown in Figure 3.39. The gain of the antenna is good at medium and higher frequencies.

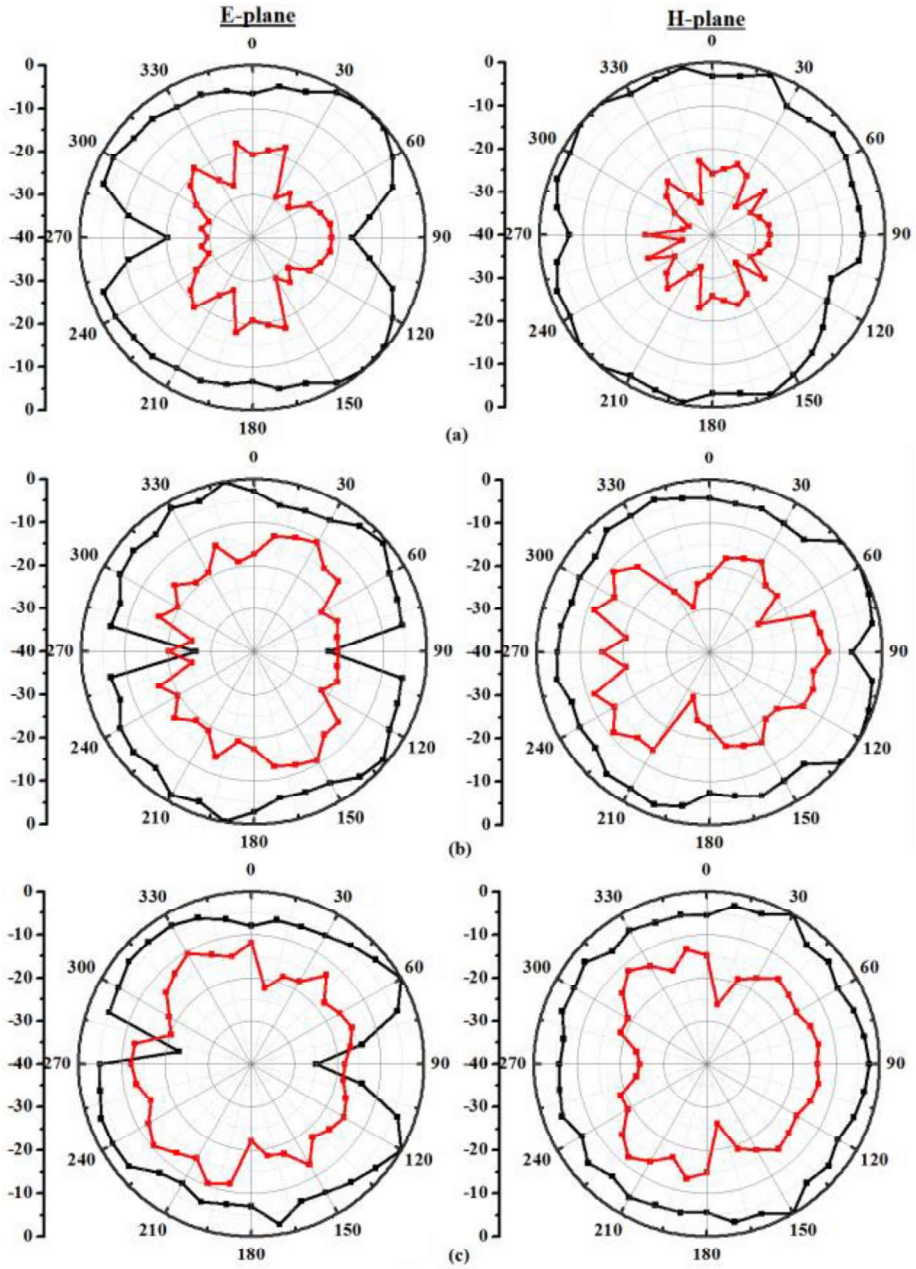

Figure 3.38: Measured radiation patterns with co-polar (—) and cross polar (—) for resonant frequencies at (a) 3.4 GHz, (b) 6.5 GHz and (c) 10.5 GHz

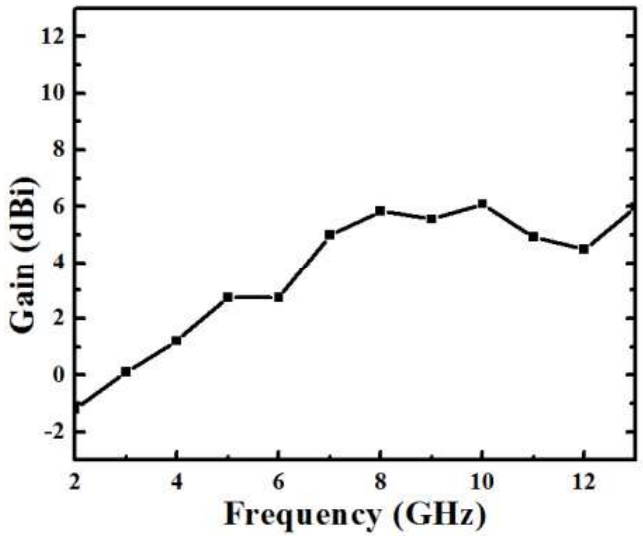

Figure 3.39: Measured Gain of proposed fractal UWB antenna

(c) Time-domain Analysis

The time domain analysis is also performed, in terms of fidelity factor to provide more insight into behaviour of the antenna. Fidelity factor measure the distortion in the input pulse at radiation. The default Gaussian signal covering the range 3.1 GHz to 10.6 GHz, generated in CST Microwave Studio, which satisfies FCC indoor and outdoor transmission limit [Koohestani *et al.*, 2013], is taken as input signal. This signal is used to calculate fidelity factor as recommended in [Wu *et al.*, 2007]. The value of fidelity factor >0.7 can be considered for well matching of radiated pulse with source pulse [Ghuang and Jeng, 2005; Chako *et al.*, 2013]. Table 3.6 shows that the fidelity factor (>0.88) which demonstrates that the radiated signal is little distorted as compared to the excited signal. This makes the proposed UWB antenna a good choice for indoor applications.

Table 3.6: Fidelity Factor of the Proposed Antenna

x-z plane, θ (°)	0	30	60	90
Fidelity Factor	0.9399	0.8880	0.8976	0.9176

3.6 Octagonal Shaped Fractal UWB Antenna Using Sierpinski Fractal Geometry

3.6.1 Antenna Design

In this section, we present a promising compact octagonal shaped fractal UWB antenna using Sierpinski fractal geometry to exploit the wideband and improved radiation property of fractal geometry. The Sierpinski fractal geometry is combined with octagonal shaped geometry to increase the effective electrical path length in a smaller area due to its space filling properties. These modifications in the geometry excite additional resonances, which enhances the bandwidth. The optimized antenna has a compact dimension of 25 mm × 16 mm. Figure 3.40 shows the geometry of the proposed UWB antenna on a rectangular FR4 epoxy substrate (W×L), having a dielectric constant of ε_r = 4.4, loss tangent tanδ = 0.023, and thickness (h) of 1.6

mm. The proposed antenna is simulated and optimized using Ansoft HFSS v.13. The selected rectangular substrate dimensions in the evolution of antenna design show wideband operability and good radiation characteristics [Tasouji *et al.*, 2013]. Hence, the rectangular dimension is preferred as initial dimension in antenna design. The patch is connected to a 50 Ω microstrip line of width (W_m) and length (L_m) for impedance matching. The ground plane of length (L_g) and width (W) is located on the other side of the substrate. The optimised dimensions of the proposed fractal UWB antenna are: L = 25 mm, W = 16 mm, R = 4.6 mm, W_m = 2.6 mm, L_m = 11.6 mm, L_g = 10.1 mm.

The proposed antenna is created by applying Sierpinski fractal at the edges of octagonal geometry. The iterative evolution of the Sierpinski fractal is shown in Figure 3.41. Here, the octagonal structure works as an initiator, and Sierpinski structure works as a generator in the evolution of initial antenna structure as shown in Figure 3.42. Figure 3.42(a) represents the initial structure without fractal application. Figure 3.42(b) and 3.42(c) shows the antenna structure with the application of first and second iteration of Sierpinski fractal at the edges of octagonal geometry, respectively. This iterative process can be repeated up to infinite, but fabrication constraints limit us up to two iterations. The application of fractal geometry excites multiple resonances and by combining them together a wideband operational bandwidth is achieved.

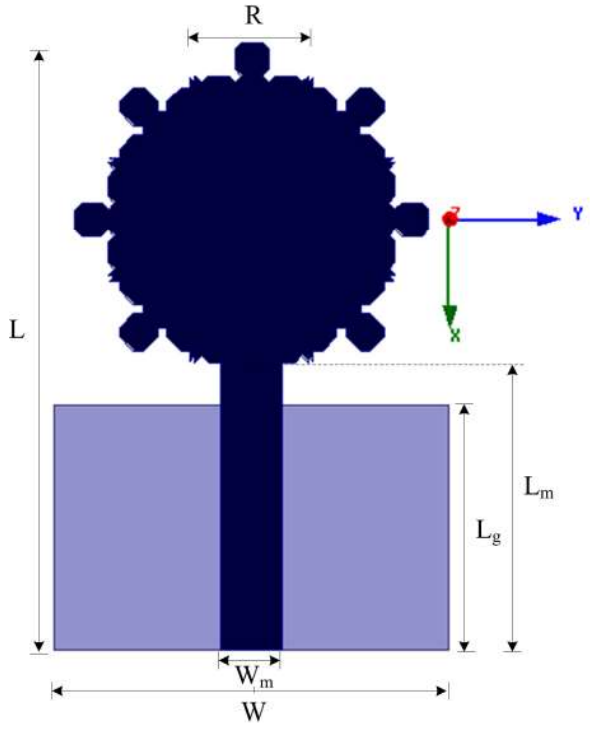

Figure 3.40: Geometry of proposed fractal UWB antenna

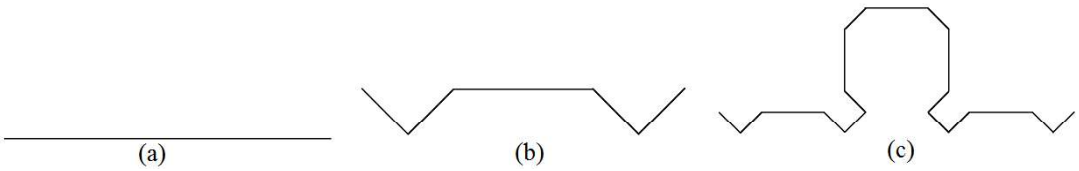

Figure 3.41: Recursive Generation of Sierpinski structure (a) Iteration-0, (b) Iteration-1 and (c) Iteration-2

Figure 3.43 displays S_{11} behaviour of the antennas generated in the evolution process of presented UWB antenna. It is observed that the lower operating resonant frequency decreases slightly with iterations due to the increase in the effective current path length. Moreover, higher operating frequency edge shows small variation with iterations. The surface current distribution of the antenna is illustrated in Figure 3.44 for better understanding of radiation mechanism. It is observed that the current is mainly distributed near the feed line, ground plane and at the edges of the Sierpinski fractal. Moreover, the current distribution at the edges of the Sierpinski fractal increases at higher frequencies which help to achieve stable radiation pattern. The fractal edges are responsible for the change in the current path which leads to enhancement in radiation characteristics of the antenna.

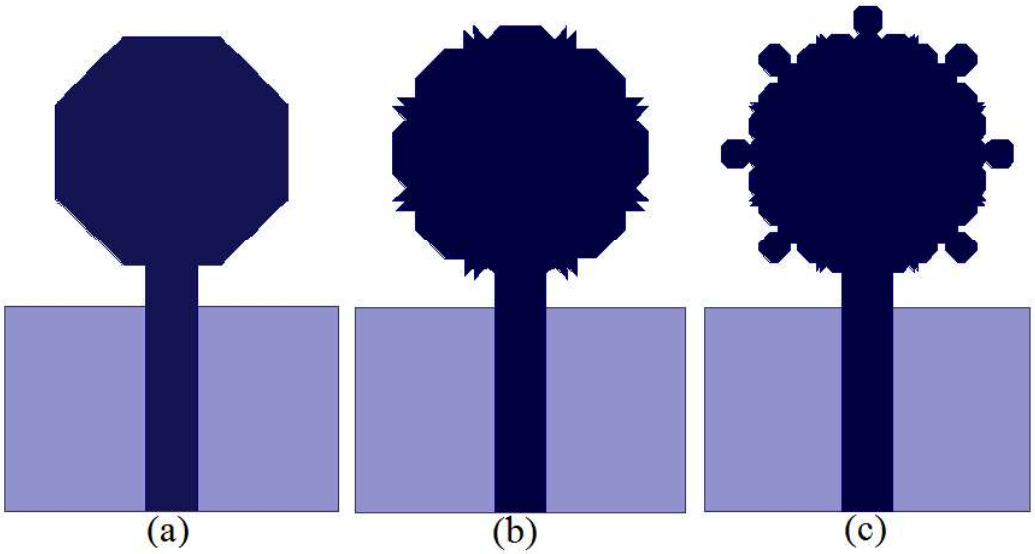

Figure 3.42: Sierpinski structure as applied to the edges of Octagonal geometry (a) Original Geometry, (b) After 1st iteration and (c) After 2nd iteration

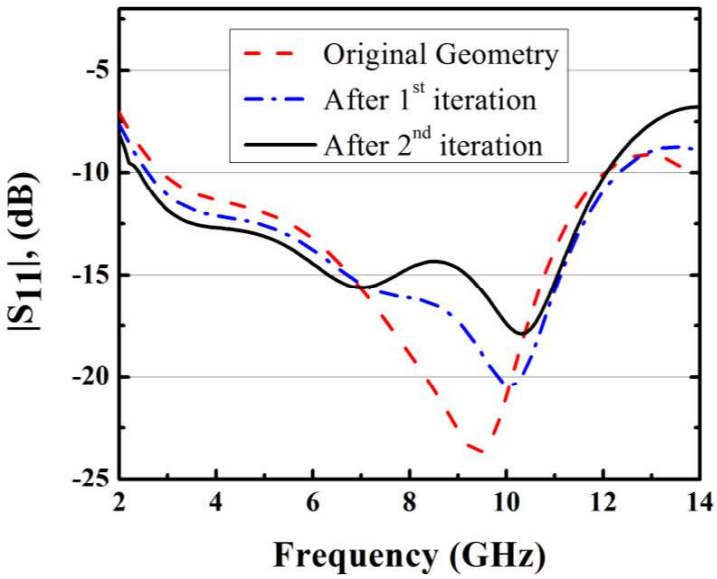

Figure 3.43: Simulated S_{11} of the antenna structures shown in Figure 3.42

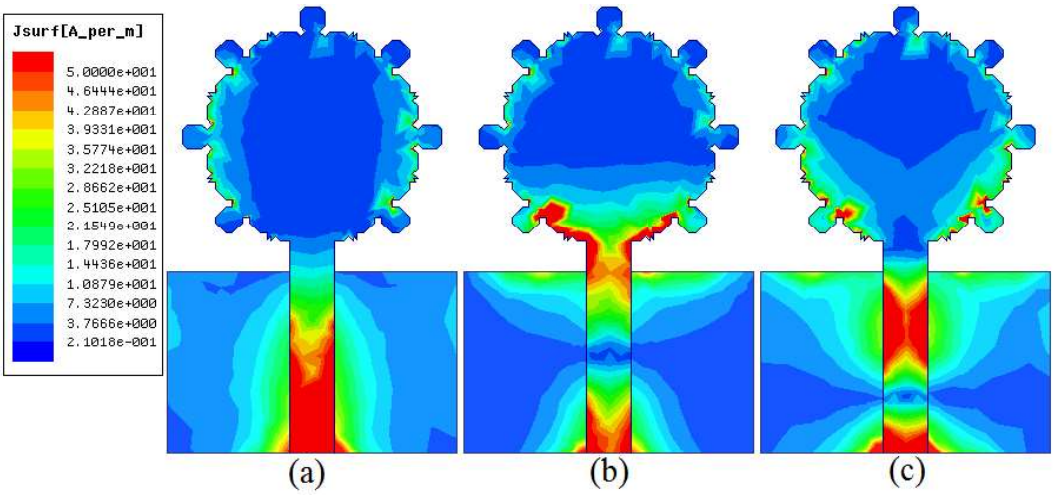

Figure 3.44: Surface current distributions at (a) 3.7 GHz, (b) 6.9 GHz and (c) 10.3 GHz

3.6.2 Results and Discussion

(a) S-parameter Result

The proposed fractal UWB antenna structure is fabricated and investigated. The photograph of the fabricated prototype is shown in Figure 3.45. The return loss measurement is performed by Agilent vector network analyser (VNA) E5071C. Figure 3.46 shows the measured and simulated return loss behaviour of the UWB antenna, and it exhibits good matching. The operating bandwidth is from 2.4 GHz to 12.1 GHz with three resonant frequencies at 3.7 GHz, 6.9 GHz and 10.3 GHz. However, the fabricated antenna exhibits operational bandwidth from 2.9 GHz to 12.3 GHz with multiple resonances. Some discrepancy is observed in the result due to the measurement environment, losses by SMA connectors and the fabrication tolerances.

Figure 3.45: Fabricated prototype of the proposed UWB antenna

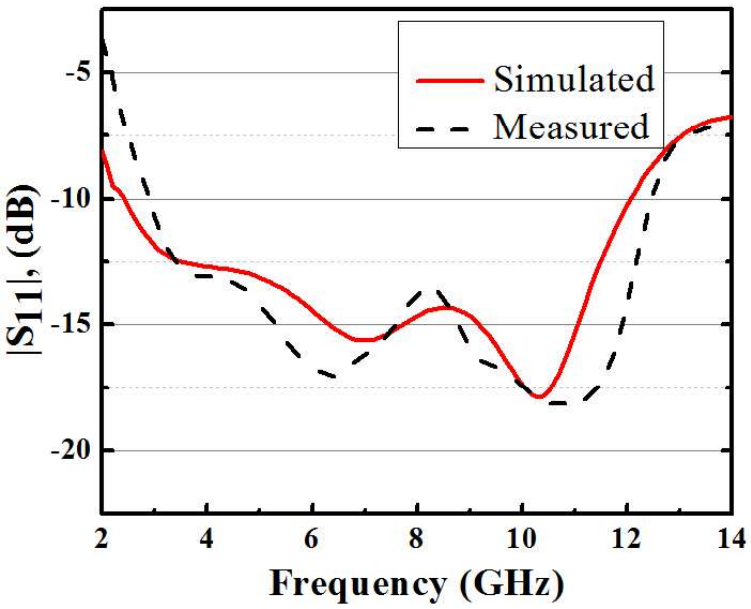

Figure 3.46: Measured and simulated return loss of antenna with various frequencies

(b) Radiation Performance

The measured gain of the proposed antenna is shown in Figure 3.47. The stable gain response is observed at middle and higher frequencies of the UWB operating range. The radiation patterns are found to be omnidirectional in H-plane (*yz*-plane) and bidirectional in E-plane (*xz*-plane), as shown in Figure 3.48. The use of fractal geometry in antenna design helps to achieve the stable radiation pattern because of current present at the fractal edges of Sierpinski geometry in monopole [Fereidoony *et al.*, 2012]. This shows good matching and lower reflection at the desired frequency.

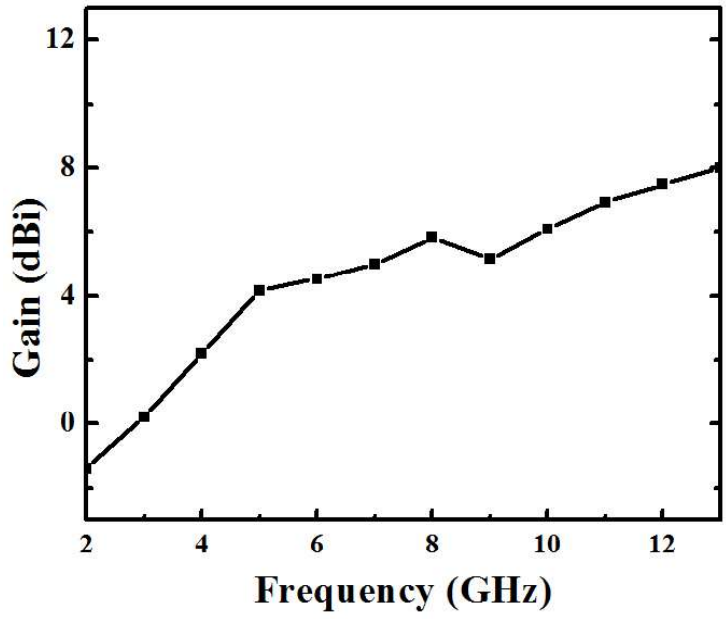

Figure 3.47: Measured Gain of the proposed fractal UWB antenna

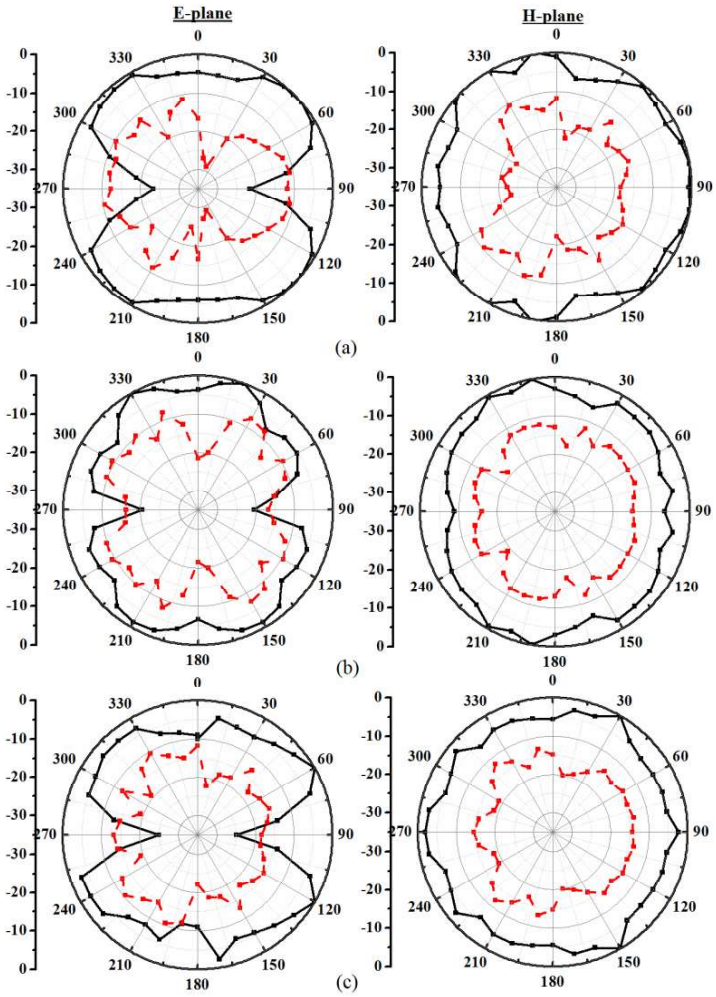

Figure 3.48: Measured radiation patterns with co-polar (—) and cross polar (- - -) for resonant frequencies at (a) 3.7 GHz, (b) 6.9 GHz and (c) 10.3 GHz

(c) Time-domain Analysis

The time-domain analysis of the antenna system, which processes short pulses of large bandwidth, is necessary. Hence, the time domain analysis is performed in terms of fidelity factor. Because of its characteristics to measure the distortion in the input pulse at the time of radiation. The default Gaussian signal, generated in CST Microwave Studio covering the UWB range 3.1 GHz to 10.6 GHz, is taken as input signal. This signal satisfies the FCC indoor and outdoor criteria, too. The fidelity factor is calculated by using the method in [Wu *et al.*, 2007], and results are given in Table 3.10. The value of fidelity factor is greater than 0.86. It illustrates that the radiated waveform is little distorted as compared with the excited signal. Hence, the proposed structure has a good pulse preserving capability. This makes the proposed antenna a good choice for UWB systems application.

Table 3.10: Fidelity Factor of the Presented Antenna

x-z plane, θ (°)	0	30	60	90
Fidelity Factor	0.8996	0.8856	0.8674	0.8612

3.7 Octagonal Shaped UWB Antenna Using Koch Fractal Geometry

3.7.1 Antenna Design

In this section, a combination of antenna technology and fractal geometry is proposed and its characteristics are investigated. It exhibits the operational impedance bandwidth over the entire UWB frequency range of 3.1 GHz to 10.6 GHz. The presented antenna has smaller dimensions and simple structure compared to antennas presented in [Guterman *et al.*, 2004; Hashemi *et al.*, 2006; Balirada *et al.*, 2011]. The Koch fractal curve is generated by using iterative function system (IFS) algorithm [Tripathi *et al.*, 2014] as shown in Eq. (3.3)-(3.6). The linear transformation matrices for Koch curve using IFS scheme can be defined as:

$$W_0 = \begin{bmatrix} \frac{1}{3} & 0 & 0 \\ 0 & \frac{1}{3} & 0 \\ 0 & 0 & 1 \end{bmatrix}, \quad W_1 = \begin{bmatrix} \frac{1}{3}\cos 60^0 & -\frac{1}{3}\sin 60^0 & \frac{1}{3} \\ \frac{1}{3}\sin 60^0 & \frac{1}{3}\cos 60^0 & 0 \\ 0 & 0 & 1 \end{bmatrix},$$

$$W_2 = \begin{bmatrix} \frac{1}{3}\cos 60^0 & \frac{1}{3}\sin 60^0 & \frac{1}{2} \\ -\frac{1}{3}\sin 60^0 & \frac{1}{3}\cos 60^0 & \frac{1}{2}\sin 60^0 \\ 0 & 0 & 1 \end{bmatrix}, \quad W_3 = \begin{bmatrix} \frac{1}{3} & 0 & \frac{2}{3} \\ 0 & \frac{1}{3} & 0 \\ 0 & 0 & 1 \end{bmatrix} \tag{3.9}$$

The first iteration divides the initial length into three equal segments and the middle segment is removed as shown in Figure 3.49. Then, middle segment is replaced by two equal segments of one-third in length. This iterative process is repeated on every segment for the generation of Koch Fractal curve. It is observed that the recursive generated Koch fractal geometry is further applied at the edges of octagonal geometry, which helps to evolve the initial antenna design as illustrated in Figure 3.50. In the evolution of the initial antenna design, octagonal geometry works as an initiator, whereas Koch fractal works as a generator. The ideal physical creation of fractal structure is not possible due to its infinite intricacy. Though, the objects with limited number of iterations can be generated considering the fabrication and complexity constraints. Thus, the proposed structure is restrained to second iteration of Koch fractal geometry. The increment in iterations represents series of similar fractal structure with different scaled geometries, which in turn leads to multiband behavior [Dhar *et al.*, 2013]. We can see from Figure 3.50 that edge of the octagonal structure is kept constant and the shape of Koch structure varies with iterations. Hence, there will be an increment in the effective area and length of the structure with the increase in iterations. Therefore, an analytical expression is required to calculate the effective dimensions of the radiator with the number of iterations. The parameters used in the design of proposed UWB antenna are as follows: θ is the base angle from the initial structure, R is the initial length, and i is the number of iteration. The variation span of angle θ is between ($-\pi/2, \pi/2$). This range of θ provides the convergence of the fractal geometry. Here, we choose $\theta = 60^0$, $R = 4.59$ mm for the iterative process. Let us assume that A_i, L_i ($i = 1, 2, 3\ldots$) be the effective area and length for a given i^{th} iteration. A_0 is the area of the initiator used. The relationship between A_i, L_i, A_0 and θ, R can be expressed as follows:

$$A_i = A_0 + \left(\frac{R}{6}\right)^2 .\tan\theta.\left[\frac{1-\left(\frac{2}{9}\left(1+\frac{\sec^2\theta}{4}\right)\right)^i}{1-\frac{2}{9}\left(1+\frac{\sec^2\theta}{4}\right)}\right] \tag{3.10}$$

$$L_i = R.\left[\frac{sec\,\theta + 2}{3}\right]^i \tag{3.11}$$

The effective area and length of the antenna radiator calculated using Eq. (3.10) and (3.12) is given in Table 3.11.

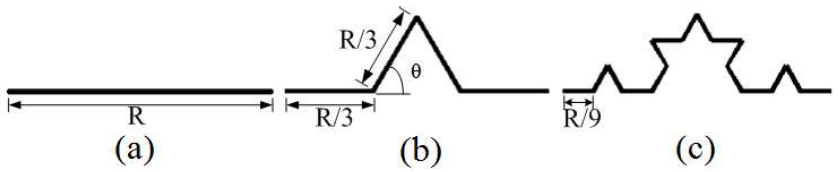

Figure 3.49: Recursive Generation of Koch structure (a) Iteration-0, (b) Iteration-1 and (c) Iteration-2

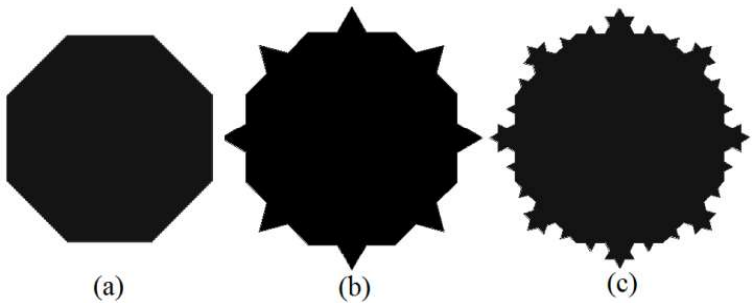

Figure 3.50: Koch structure as applied to the edges of Octagonal geometry (a) Initiator, (b) After 1st iteration, (c) After 2nd iteration

Table 3.11: The effective area and length of the proposed UWB antenna

Parameters	Iteration-0	Iteration-1	Iteration-2
Effective Area (mm^2)	101.72	109.82	113.41
Effective Length (mm)	36.72	48.96	53.04

It is noticed from Table 3.8 that with the increment in iterations the overall area as well as path length of radiator is increased. Moreover, the higher iteration of the Koch structure generates multiple resonant frequencies due to its fractal properties [Daotie *et al.*, 2012]. Figure 3.51 shows the proposed antenna with a fractal radiator and a rectangular ground plane. The proposed antenna is designed and its characteristics are investigated by Ansoft HFSS v.13. The proposed antenna design is simulated on a rectangular substrate (W×L), FR4, having a dielectric constant of ε_r = 4.4, loss tangent tanδ = 0.02, and thickness of 1.6 mm. The rectangular substrate is chosen for the basic design in the evolution of proposed UWB antenna because of its wideband operability and good radiation characteristics [Tasouji *et al.*, 2013]. The patch is connected to a 50 Ω microstrip line of width (W_m) for impedance matching. The ground plane is positioned on the other side of the substrate having length (L_g) and width (W). The optimized design parameters of proposed octagonal fractal UWB antenna are listed in Table 3.9.

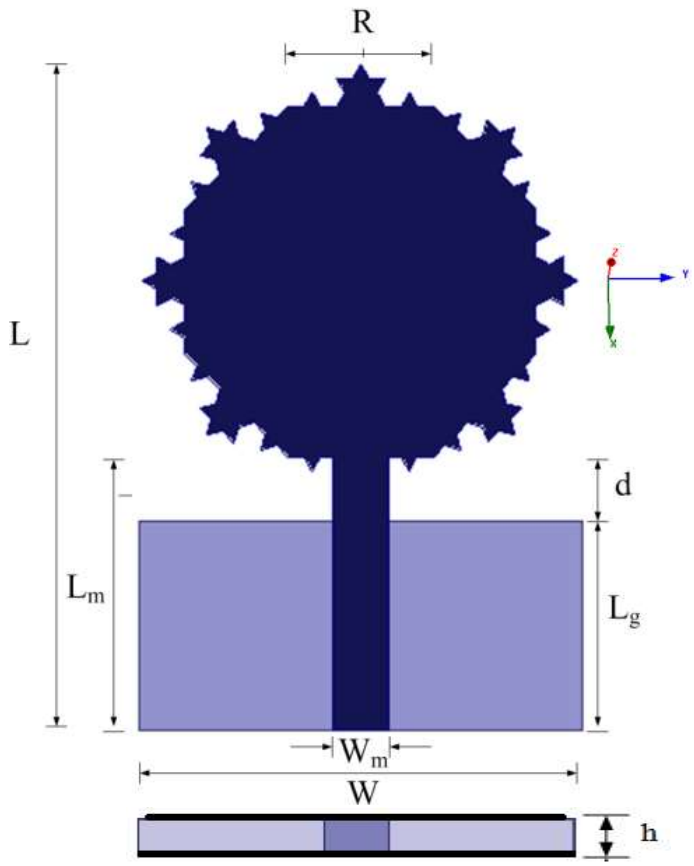

Figure 3.51: Geometry of the proposed Octagonal fractal antenna

Table 3.9: Optimized geometrical parameter of the proposed UWB antenna

Parameters	Dimensions	Parameters	Dimensions
L	23.5	d	2.0
W	15.0	L_g	9.0
R	4.59	W_m	2.2
h	1.6	L_m	11.0

3.7.2 Results and Discussion

(a) S-parameter Result

The proposed octagonal fractal UWB antenna is fabricated and its characteristics are investigated using Agilent E5071C vector network analyzer (VNA). The fabricated prototype of the proposed antenna is shown in Figure 3.52. The measured and simulated return loss of the UWB antenna is shown in Figure 3.53. The measured result shows a good match with simulated results in the entire UWB frequency range. It is observed that measured operating range is from 2.5-12.2 GHz with three resonant frequencies in the UWB range. The experimental results show that mismatch with simulated result at the lower operating frequency around 3 GHz is less, which implies that the impedance matching of the antenna is less dependent on the ground plane [Ahmed, 2011]. Some discrepancy in result is observed due to the measurement environment, losses introduced by SMA connectors and the fabrication tolerances.

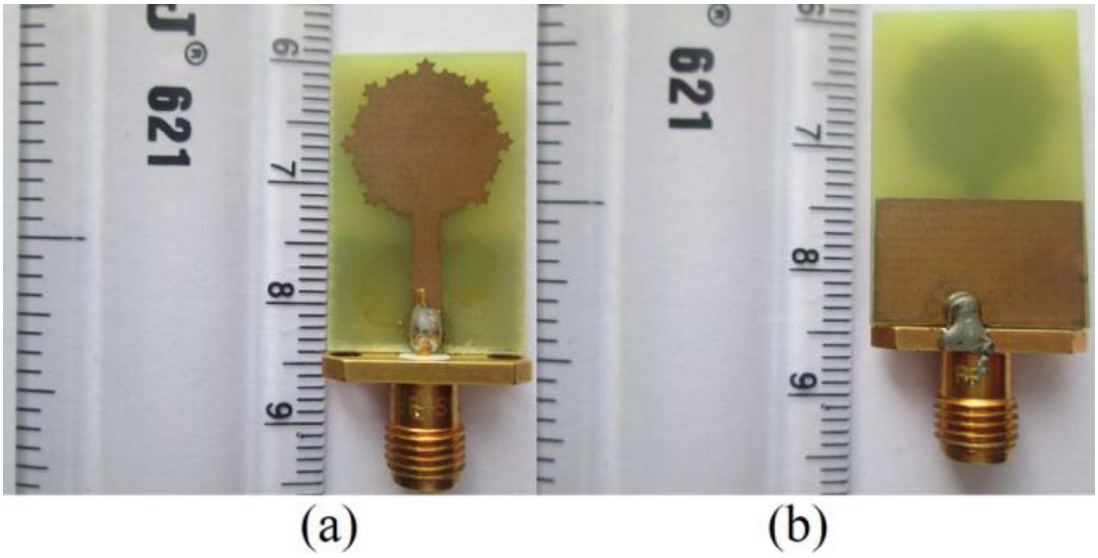

Figure 3.52: Photograph of the fabricated antenna (a) Front view (b) Bottom view

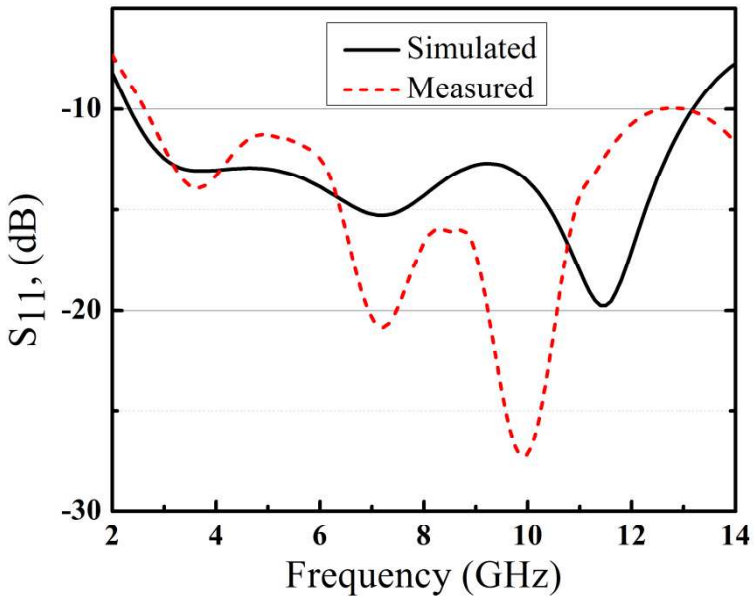

Figure 3.53: Simulated and measured return loss of antenna at various frequencies

(b) Input Impedance Performance

The real and imaginary impedance of the proposed antenna is shown in Figure 3.54. The impedance matching at the higher frequencies is relatively better compared to the lower frequencies. The input reactance in the UWB frequency range changes between -20 to 25 Ω. This small variation range indicates the broadband nature of the antenna. It is relevant to see that the flat response of both the real and imaginary parts of the input impedance resulting in a broadband bandwidth from 2.3-13.2 GHz. The real input impedance of the proposed fractal UWB antenna approaches to 50 Ω at resonant frequencies 3.6 GHz, 7.2 GHz and 11.5 GHz respectively. The acceptable impedance variation shows that the proposed antenna is suitable for entire UWB frequency spectrum.

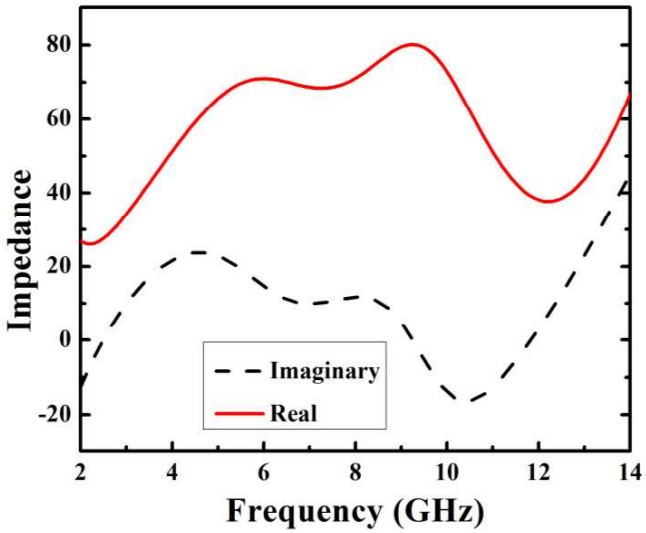

Figure 3.54: Simulated result of real and imaginary impedance

(c) Radiation Performance

Figure 3.55 displays the measured gain of the proposed antenna. It indicates that antenna gain is low in the low frequency domain, due to its smaller dimension, which indicates the tradeoff between gain bandwidth and its dimension. In the middle frequency range the variation range of gain is between 2 to 3.5 dBi. At higher frequencies, the decrement in the gain is observed. Figure 3.56 shows the measured radiation pattern of the antenna. It deals with the antenna's directional behavior for constant radial distance and frequency in the far field region using principal *E*-plane (*xz*-plane) and *H*-plane (*yz*-plane) patterns [Balanis, 2005]. The radiation patterns are found to be omnidirectional in H-plane and bidirectional in E-plane with low cross-polarization at the resonant frequencies of 3.6 GHz, 7.2 GHz and 11.5 GHz. At higher frequencies, the variation in the radiation pattern is observed due to the reflection at edges from the fractal structure and the change in the current nature. The current nature changes from standing wave pattern at lower frequencies to a travelling wave pattern at higher frequencies [Allen *et al.*, 2007].

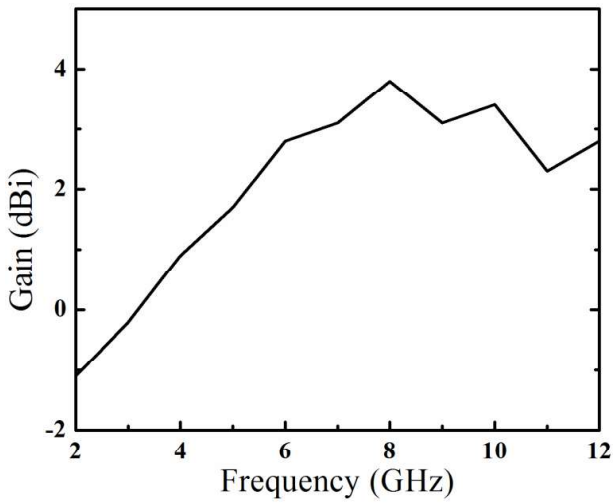

Figure 3.55: Measured gain of the proposed antenna as a function of frequency

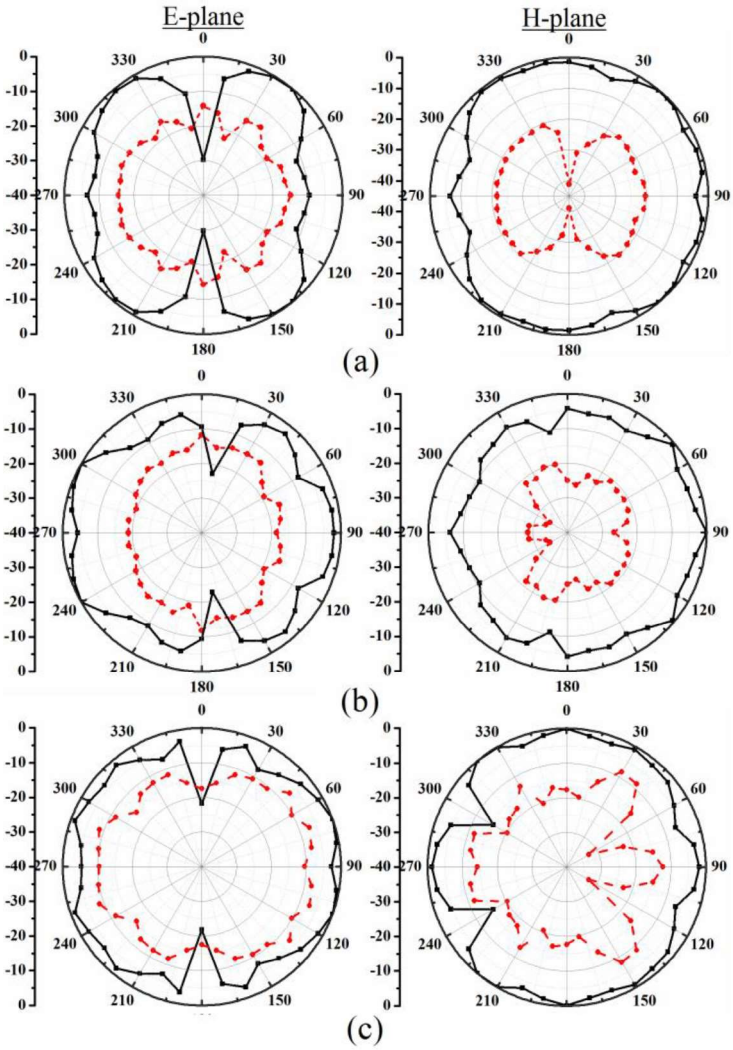

Figure 3.56: Radiation patterns for the proposed fractal UWB antenna with co-polar (——) and cross polar (- - -) at resonant frequencies (a) 3.6 GHz, (b) 7.2 GHz and (c) 11.5 GHz

(d) Time-domain Analysis

The time-domain analysis of antennas which processes short pulses of large bandwidth provides a better understanding of antenna performance. The proposed antenna analysis, in terms of fidelity factor, determines the level of distortion introduced by the antenna to its input signal. The fidelity factor is defined mathematically as:

$$\rho = \max_{\tau}\left\{\left|\frac{\int S(t)\,R(t-\tau)\,dt}{\sqrt{\int S^2(t)\,dt}\sqrt{R^2(t)\,dt}}\right|\right\} \tag{3.12}$$

where, τ is delay, S(t) is the source pulse, and R(t) is the received pulse. The cross correlation is performed on the source signal and received signal, and maximum is computed. The default Gaussian modulated pulse (3.1-10.6 GHz) of CST is used for time-domain analysis of proposed antenna. This pulse satisfies the regulation criteria of FCC indoor and outdoor power mask [Koohestani *et al.*, 2013]. The fidelity factor is calculated for elevation and azimuthal plane, as suggested in [Wu *et al.*, 2007]. The probe is defined at a distance of 400 mm for every 30^0 from 0^0 to 90^0. This selected large distance helps to accomplish the far field criteria. It is almost four

times the wavelength of the lower UWB operating frequency. The value of fidelity factor >0.7 can be considered for well matching of radiated pulse with source pulse [Ghuang and Jeng, 2005; Chako *et al.*, 2013]. Table 3.7 illustrates that the fidelity factor variation is in the range of 0.81-0.96 for Koch geometry. Thus, the proposed antenna structure does not distort the incident pulse significantly, which makes it a suitable choice for UWB applications.

Table 3.7: Fidelity Factor of proposed Fractal Antenna

(*x*-z) plane	θ=0°, φ=0°	θ=30°, φ=0°	θ=60°, φ=0°	θ=90°, φ=0°
	0.8467	0.8114	0.8316	0.8386
(*x*-y) plane	φ=0°, θ=90°	φ=30°, θ=90°	φ=60°, θ=90°	φ=90°, θ=90°
	0.9606	0.9484	0.9486	0.9669

3.8 Hexagonal Shaped Fractal Koch UWB Antenna With Fractal Ground Plane

3.8.1 Antenna Design

In this section, a novel design approach for bandwidth enhancement of UWB antenna is presented. In this design fractal Koch geometry, as shown in Figure 3.57 and generated using Eq. (3.3)-(3.9), is applied at the edges of hexagonal monopole as well as at the ground plane. The proposed antenna is generated by combining the Koch fractal and the hexagonal geometry. The Koch fractal geometry is further applied to the edges of the hexagonal geometry. Here, this selected hexagonal shape and Koch fractal works as a initiator and generator, respectively, in the evolution of initial antenna design.

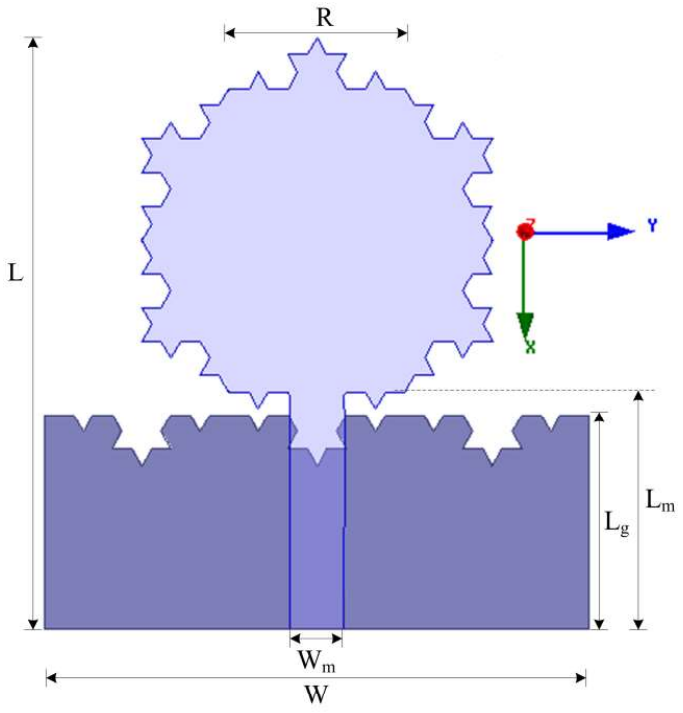

Figure 3.57: The optimized structure of the proposed fractal UWB antenna

The initial structure of the antenna without application of fractal geometry is shown in Figure 3.58(a). Figure 3.58(b) and (c) display the structures of the antenna after applying first and second iteration of the Koch geometry at the edges of monopole, respectively. The introduction of Koch geometry in the ground plane of antenna structure is shown in Figure 3.58(d). The proposed structures (with and without Koch fractal) is simulated using HFSS v.13 on a rectangular substrate (W × L), FR4, having a dielectric constant (ε_r) 4.4, loss tangent (tanδ) 0.023, and thickness (h) 1.6 mm. The rectangular substrate is selected due to two reasons. Firstly, rectangular structure of the substrate offers wideband operability. Secondly, it helps to achieve good radiation property [Tasouji *et al.*, 2013]. The hexagonal monopole with the edges of length R is connected to a 50 Ω microstrip line of width (W_m) and length (L_m) for impedance matching. Ground plane is positioned on the other side of the substrate having length (L_g) and width (W). The values of above mentioned parameters are same as given in Table 3.11.

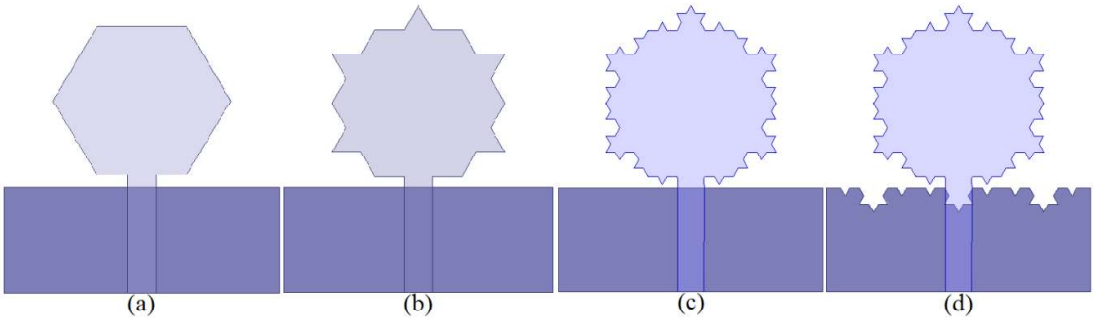

Figure 3.58: Evolution of the fractal UWB antenna with application of Koch geometry (a) Antenna-0, (b) Antenna-1, (c) Antenna-2 and (d) Antenna-3

Table 3.11: Optimized geometrical parameter of the proposed UWB antenna

Parameters	Dimensions (mm)	Parameters	Dimensions (mm)
L	31.0	L_m	12.0
W	28.0	W_m	3.0
R	9.0	L_g	11.1

The S_{11} for the various antenna structures generated in the evolution process are shown in Figure 3.59. It is observed that addition of Koch geometry with monopole increases the electrical path length of monopole. Moreover, fractal monopole possesses greater perimeter length in a smaller area as compared to other geometries such as circle, ellipse, hexagon, etc. The lower operating frequency is changes slightly with the increase in iteration of Koch geometry. These modifications in the geometry improve the S_{11} characteristics significantly in the mid as well as high frequency ranges of UWB spectrum. The fractal geometry produces multiple resonances and by combining these resonances wideband bandwidth is achieved. The introduction of Koch geometry into the ground plane further improves bandwidth because of change in the electrical path length and excitation of additional resonances. Tuning the ground plane has been useful to increase bandwidth of the antenna elements [Abedin and Ali, 2003; Anguera *et al.*, 2010; Sanz-Izquierdo *et al.*, 2004; Cabedo *et al.*, 2009], this helps to achieve the operational bandwidth up to 122%. The optimized structure of the UWB antenna has the operational bandwidth from 3 GHz to 12.8 GHz with three resonant frequencies at 4.3 GHz, 7.2 GHz, and 10 GHz and its optimized parameters are shown in Table 3.11.

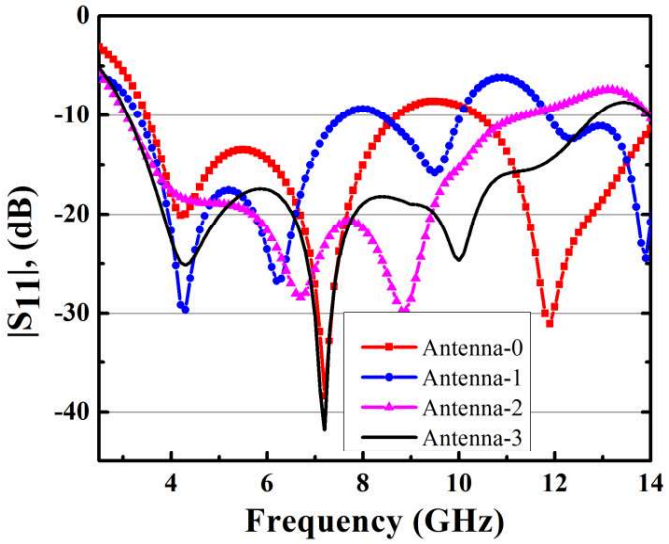

Figure 3.59: Simulated $|S_{11}|$ of the different antenna structures in the evolution

The surface current density distribution on the fractal monopole and fractal ground plane at resonant frequencies is shown in Figure 3.60. At 4.3 GHz resonant frequency, the surface current distribution is mainly concentrated at the edges of the fractal structure of monopole and ground as can be seen from Figure 3.60(a). This shows that Koch fractal affects the impedance matching significantly at lower frequencies. Figure 3.60(b) shows the surface current distribution at 7.2 GHz. It is observed that the fractal edges of the monopole and lower portion of the ground plane has more effect on the impedance matching. At 10 GHz resonant frequency, the surface current distribution is shown in Figure 3.60(c), which illustrates that the current distribution intensity is significant at the fractal edges of the ground plane and junction of the monopole and feed. This demonstrates that the application of the Koch structure in the ground plane has more significant impact at higher frequencies as compared to lower frequencies, which is also reflected in the S_{11} behavior as depicted in Figure 3.58. The surface current distribution at monopole is more uniform at lower frequency as compared to higher frequency due to the change in nature of the current [Allen *et al.*, 2007]. At lower frequencies, the wavelength of the EM waves is long and small segments of the Koch structure contribute less in the overall radiations. However, at higher frequencies, the segment dimensions become comparable to the wavelength, which enhance the radiation characteristic significantly [Balirada *et al.*, 1998].

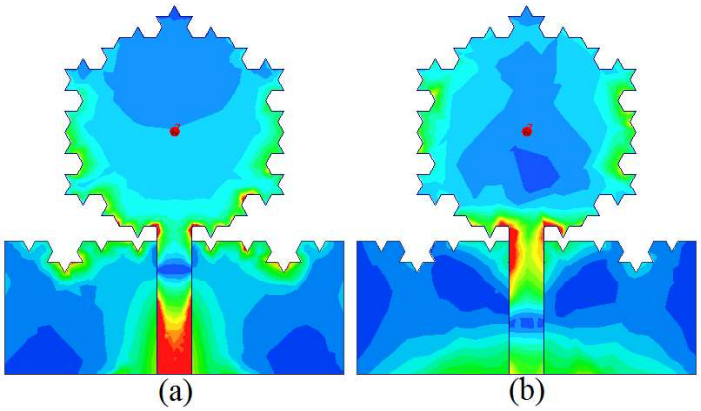

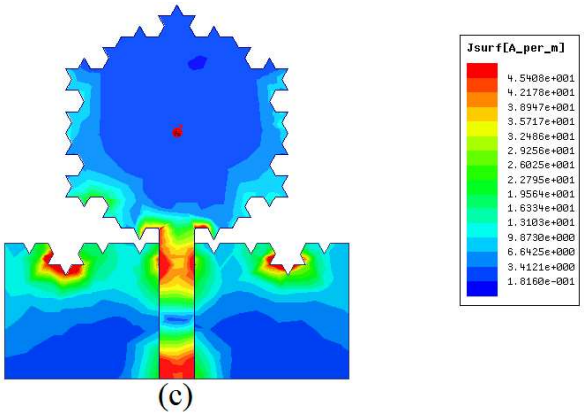

Figure 3.60: Surface current distribution of the fractal UWB antenna at (a) 4.3 GHz, (b) 7.2 GHz and (c) 10 GHz

3.8.2 Results and Discussion

(a) S-parameter Result

The prototype of the proposed UWB antenna structure is fabricated and its characteristic is investigated. The measurement is performed by Agilent Vector Network Analyzer E5071C. The top and bottom view of the fabricated prototype of the proposed antenna is shown in Figure 3.61. Figure 3.62 shows the simulated and measured S_{11} results. The measured results show almost entire UWB bandwidth from 3.4 GHz to 13 GHz with multiple resonant frequencies. The multiple resonant frequencies are observed due to the introduction of Koch geometry in the antenna design. However, some differences have been observed due to the measurement environment, losses introduced by SMA connectors and the fabrication tolerances.

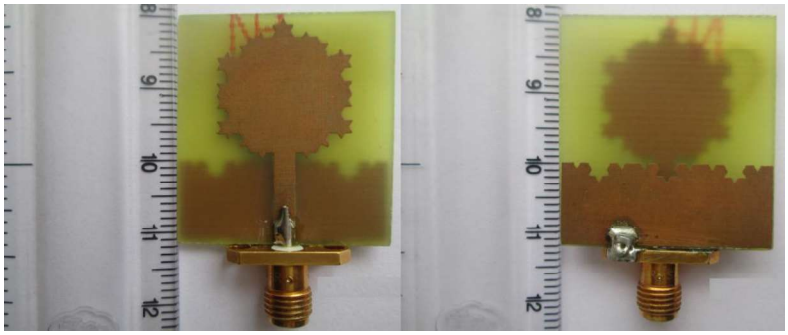

Figure 3.61: Fabricated prototype of the antenna (a) Top view and (b) Bottom view

(b) Input Impedance Performance

The simulated real and imaginary impedance of the fractal UWB antenna is shown in Figure 3.63. The impedance matching is good throughout UWB operating frequency range. It is observed that at the resonant frequencies real input impedance approaches to 50Ω. The input reactance varies between -15Ω to 15Ω in the UWB range. It illustrates the broadband nature of the proposed UWB antenna. It is relevant to see that the flat response of both the real and imaginary part of the input impedance resulting in a broadband bandwidth from 3 GHz to 12.8 GHz. The variations in the impedance over the UWB operating ranges are in acceptable range.

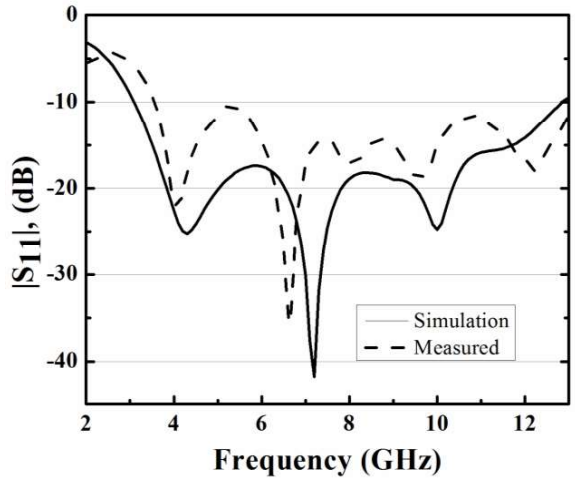

Figure 3.62: Measured and simulated $|S_{11}|$ of the proposed antenna

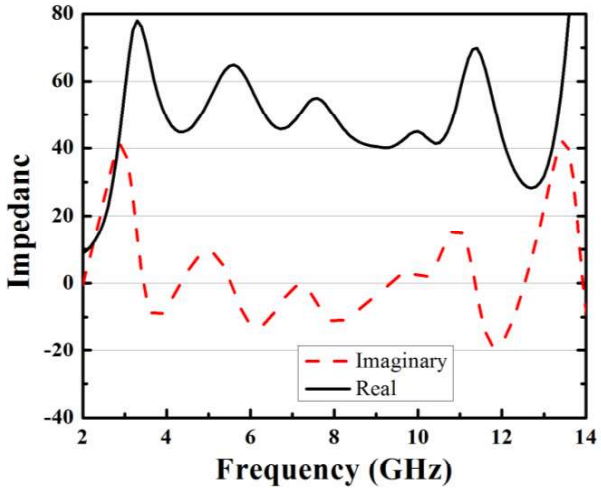

Figure 3.63: Simulated real and imaginary impedance of the proposed antenna

(c) Radiation Performance

Figure 3.64 shows the measured radiation pattern of the proposed antenna at 4.3 GHz, 7.2 GHz, and 10 GHz in both E-plane (*xz* plane) and H-plane (*yz* plane). According to the figures, H-plane pattern is nearly omnidirectional, whereas E-plane pattern is bi-directional. The cross-polarization component in the E-plane as well as in the H-plane inevitably increases with the increase in resonant frequency. It is observed that the radiation pattern at higher resonant frequency shows small deviations as compared to lower resonant frequency due to the reflection at edges from the fractal antenna structure and the change in the nature of the current from standing wave pattern at lower frequencies to a travelling wave pattern at higher frequencies [Allen *et al.*, 2007]. The surface current distribution intensity at the fractal edges of the Koch geometry is significant at low and high resonant frequencies. The fractal curves and bends causes for the change in the current path, which supports to enhance the radiation characteristics of the antenna [Fereidoony *et al.*, 2012]. This helps to improve the antenna gain. Figure 3.65 shows the gain of the proposed antenna on *xy*-plane ($\theta=90^0$, $\varphi=0^0$). It shows that the gain varies between 6 dBi to 4 dBi in the UWB frequency range. At higher frequencies above 6 GHz, gain of the antenna increases steadily.

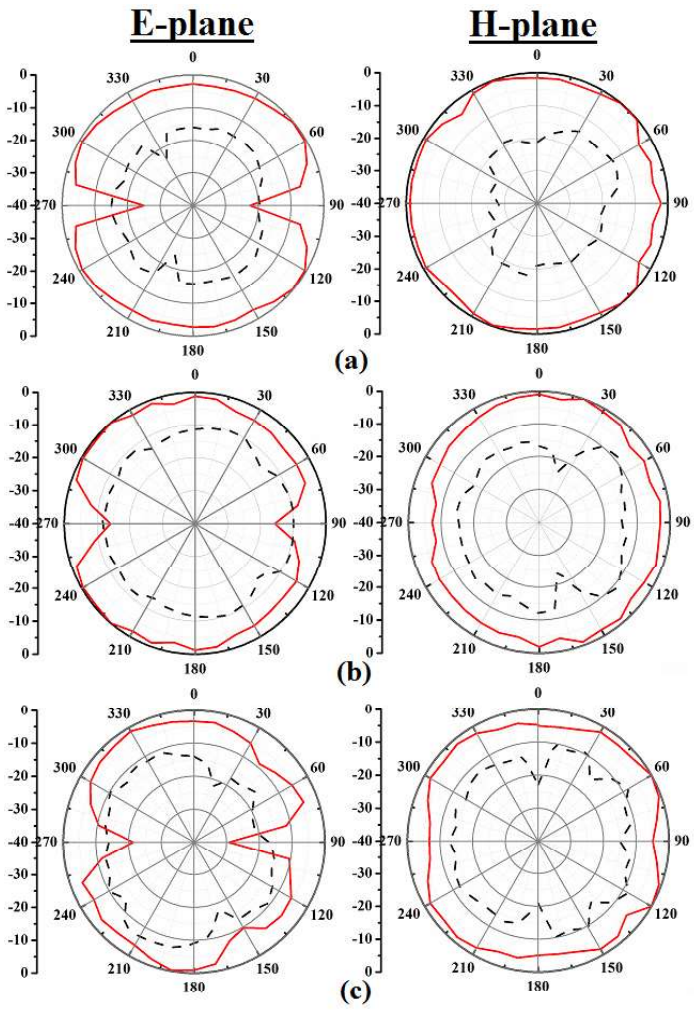

Figure 3.64: Measured radiation pattern with co-polarization (—) and cross-polarization (---) at (a) 4.3 GHz, (b) 7.2 GHz and (c) 10 GHz

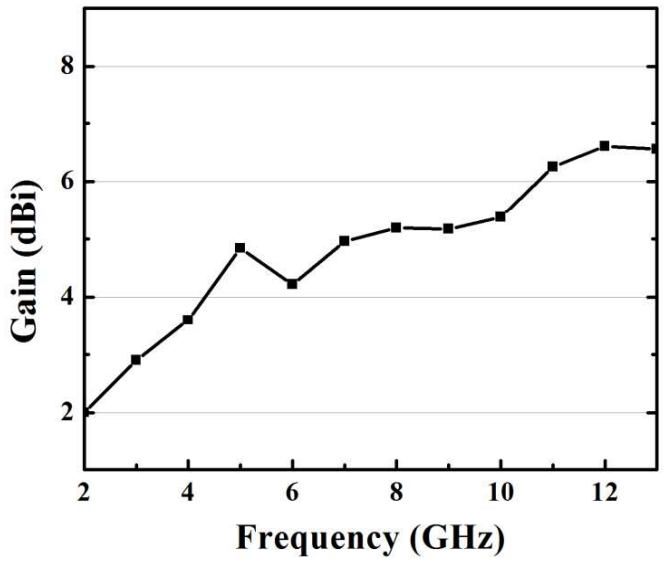

Figure 3.65: Measured Gain of the proposed antenna versus frequency

(d) Time-domain Analysis

The frequency domain characteristic of antennas which processes short pulses of large bandwidth becomes cumbersome. In such cases, time domain characteristic provides a better understanding of antenna performance. The proposed antenna is analyzed using fidelity factor. The time-domain characteristics of proposed antenna is analyzed using CST default Gaussian modulated pulse, with a spectrum range 3.1-10.6 GHz. This pulse satisfies the FCC indoor and outdoor power mask [Koohestani *et al.*, 2013]. The input signal is given to the antenna and the received pulse is obtained by means of a virtual probe as suggested in [Wu *et al.*, 2007]. Fidelity factor is calculated for elevation and azimuthal plane. The probe is defined at a distance of 400 mm for every 10^0 from 0^0 to 90^0. The chosen distance is large enough to accomplish the far field criteria, nearly four times the wavelength of the lower UWB operating frequency. The value of fidelity factor >0.7 can be considered for well matching of radiated pulse with source pulse [Ghuang and Jeng, 2005; Chako *et al.*, 2013]. Table 3.12 shows the fidelity factor variation in the range of 0.81 to 0.92. The results show that the proposed antenna structure does not distort the incident pulse significantly, which makes it a suitable choice for UWB application.

Table 3.12: Fidelity factor of the proposed antenna

Probe positions (x-z plane)	Fidelity Factor	Probe positions (x-y plane)	Fidelity Factor
$\theta = 0^o, \varphi = 0^o$	0.8918	$\varphi = 0^o, \theta = 90^o$	0.8165
$\theta = 30^o, \varphi = 0^o$	0.8778	$\varphi = 30^o, \theta = 90^o$	0.8537
$\theta = 60^o, \varphi = 0^o$	0.8487	$\varphi = 60^o, \theta = 90^o$	0.8819
$\theta = 90^o, \varphi = 0^o$	0.8371	$\varphi = 90^o, \theta = 90^o$	0.9183

Table 3.13: Comparison of the proposed work with others presented in the literature

Antennas	Dimensions (mm×mm×mm)	Bandwidth (GHz)	Maximum Gain (dBi)
Work in Section 3.2	23.5 × 26.5 × 1.6	1.4-10.4	3.1
Work in Section 3.3	19 × 15 × 0.78	3.1-11.6	3.4
Work in Section 3.4	16.5 × 13.5 × 0.78	3.1-10.6	2.2
Work in Section 3.5	25.5 × 16 × 1.6	2.1-12	5.8
Work in Section 3.6	25 × 16.5 × 1.6	2.4-12.1	5.2
Work in Section 3.7	23.5 × 15 × 1.6	2.5-12.2	4.8
Work in Section 3.8	31 × 28 × 1.6	3-12.8	6.1
Hashemi *et al.*, 2006	60 × 40 × 1.6	2-2.3, 3.6-3.9, 4.5-6.1, 7-7.5, 9.2-9.8	8.8
Oraizi et al., 2011	25 × 20 × 1.6	3.4-13	4.4
Li *et al.*, 2013	26 × 21 × 1.6	2.8-11	4.5
Pourahmadazar et al., 2011	25 × 25 × 1	2.8-11	2.6
Patnam, 2008	36 × 22.25 × 1.6	2.64 – 11.14	2.5

3.9 Summary

In this chapter, different fractal geometry such as Minkowski like, Minkowski, Sierpinski and Koch are used in the UWB antenna design to achieve the desired miniaturization, wide impedance bandwidth and stable radiation pattern. The application of

Minkowski like fractal structure have been studied for designing novel UWB antenna in the first design and its properties are investigated. The applications of Minkowski like geometry not only increase the effective length but also provide good wideband phenomena. The repetition of Minkowski like segments in the radiator provides multiple prominent resonant frequencies.

Moreover, Minkowski like fractal geometry is applied at the edges of hexagonal and octagonal shaped geometry in the second and third design, respectively, and its characteristics are studied. It is observed that the introduction of Minkowski like fractal geometry at the edges of hexagonal and octagonal geometries provides the compactness in dimension as well as it increases the effective electrical path length. Further, modifications in the ground plane by introducing multiple notches generate additional resonances at higher frequencies and disperse surface current due to the generation of new path, which helps to achieve the desired UWB frequency band i.e. from 3.1 GHz – 10.6 GHz.

The fourth and fifth design show Minkowski and Sierpinski fractal geometry based compact UWB antennas, respectively. The application of Minkowski and Sierpinski fractal geometry increases the effective length and miniaturizes the antenna size drastically, which helps to achieve the desired compactness in design. The time domain analysis shows nearly constant fidelity factor, which demonstrate good pulse preserving capability of the presented antennas.

The Koch fractal structure has been studied for designing novel UWB antenna in the sixth and seventh design and its properties are investigated. The Koch fractal is applied at the edges of the monopole in the sixth design. Moreover, Koch fractal is applied at the edges of monopole and at the ground plane in the seventh design. The introduction of Koch fractal in the ground plane excites additional resonances, which in turn leads to bandwidth improvement up to 122%. In addition, the fractal nature of the antenna also facilitates to get the stable radiation pattern at higher frequencies. An analytical formula is provided to calculate the effective length and area of the antenna structure for a given iteration order. Furthermore, a comparative study between presented work in the chapter and the work available in the literature is also provided, in the Table 3.13, in terms of antenna characteristics parameters such as dimension, bandwidth and gain.

The design approach presented in this chapter provides a good solution for wideband compact fractal antennas with good radiation characteristics, which can be used for wireless personal area network (WPAN), wireless body area network (WBAN), etc.

…